ANL-7880
Reactor Technology

ARGONNE NATIONAL LABORATORY
9700 South Cass Avenue
Argonne, Illinois 60439

METHOD FOR CALCULATING DISTRIBUTIONS OF FLUX, POWER, AND BURNUP IN OXIDE SUBASSEMBLIES IRRADIATED IN EBR-II

by

G. H. Golden and L. B. Miller

EBR-II Project

February 1972

DISCLAIMER

TABLE OF CONTENTS

TABLE OF CONTENTS

LIST OF FIGURES

LIST OF TABLES

NOMENCLATURE ➧

NOMENCLATURE

Take the active length of an element irradiated in EBR-II to be divided into 20 equal nodes. The peak flux and fission densities are found in node 10, just below the midplane.

N	Total number of configurations chosen to represent an irradiation
t	Total irradiation time, sec
M_i	Number of megawatt-days of irradiation for X-Y group i, i = 1, ..., N
P_i	Nominal reactor power for X-Y group i, i = 1, ..., N
σ_{fj}^{m}	jth-group microscopic fission cross section of heavy nuclide m, cm^2
$\varphi_j(k)$	jth-group absolute neutron flux in axial node k, neutrons/cm^2-sec
J	Total number of neutron-energy groups
$\sum_J \sigma_{fj}^{m} \varphi_j(k)$	Fission rate per atom of heavy nuclide m, summed over J groups in axial node k, fissions/atom-sec
N_0	Avogadro's number, 6.02253×10^{23} atoms/mole
A_m	Atomic weight of heavy nuclide m
$r_m(k)$	Absolute fission density of heavy nuclide m in axial node k, fissions/g-sec
$\beta_{mn}(k)$	Mass, in grams, of heavy nuclide m burned per initial gram in axial node k, nth iteration
$W_m(k)$	Initial mass of heavy nuclide m in axial node k, g
$\overline{W_m(k)}$	Midlife mass of heavy nuclide m in axial node k, g
$BU(k)$	Total burnup in axial node k
$W_s(k)$	Mass of stainless steel in axial node k, g
$P_{\gamma h}(k)$	Deposition of gamma power in heavy nuclides in axial node k, MeV/g-sec
$P_{\gamma s}(k)$	Deposition of gamma power in stainless steel in axial node k, MeV/g-sec
$P(k)$	Total midlife power deposition in axial node k, Btu/hr
E_m	Total kinetic and β-particle energy deposited per atom of heavy nuclide m fissioned, MeV/fission
K	5.4678×10^{-13} Btu/hr/(MeV/sec)
$\overline{(\text{MeV/fission})}_k$	Effective MeV/fission in axial node k, defined by Eq. B.2 (Appendix B)
D_{sj}	Diffusion coefficient for group j in subassembly s, cm
B_z^2	Transverse buckling, cm^{-2}

METHOD FOR CALCULATING DISTRIBUTIONS OF FLUX, POWER, AND BURNUP IN OXIDE SUBASSEMBLIES IRRADIATED IN EBR-II

by

G. H. Golden and L. B. Miller

ABSTRACT

A method for calculating the axial distributions of flux, power, and burnup in LMFBR mixed-oxide fuel elements irradiated in EBR-II has been developed. Peak absolute fluxes and fission densities for ^{235}U, ^{238}U, ^{239}Pu, and ^{240}Pu are obtained from transport-theory calculations in X-Y geometry for specific run configurations in EBR-II. These calculations display global and local variations in flux in the reactor. Relative axial distributions are obtained from transport-theory calculations in R-Z geometry. A procedure for accounting for burnup of the heavy nuclides is given. The effective MeV/fission to be used to convert rate of total fission to power is calculated for a subassembly of 19 mixed-oxide elements in row 4 and a subassembly of 37 mixed-oxide elements in row 5 of EBR-II. The elements studied were C17 and C1 in subassemblies X012 and X012A, and F3B3 and 011 in subassembly X040A.

I. INTRODUCTION

The prototypal LMFBR fuel element is a UO_2-PuO_2 mixture clad with a stainless steel tube. The in-reactor performance of many such mixed-oxide elements is being investigated by irradiating them in the Experimental Breeder Reactor II (EBR-II). This performance is strongly affected by swelling and creep of the cladding. It is also affected by swelling, cracking, and restructuring of the fuel; release of fission gas from the fuel; and migration of fissile material in the fuel. A detailed understanding of these effects and how they interact is therefore essential to the design of a safe, reliable, and economical oxide fuel element for LMFBR's.

Individual effects, such as cladding swelling, are treated by semi-theoretical[1] or empirical[2] models. Interaction of the individual effects is treated by incorporating them into computerized mechanical models, such as the LIFE code.[3] Two major aspects of the development of these codes for fuel lifetime are:

1. Testing models of individual effects, such as cladding swelling and fuel restructuring, by comparison with observed effects.

2. Testing the codes by benchmark irradiation experiments.

This testing requires that the neutron flux and power distributions in each irradiated element of interest be characterized.

Until recently, such characterization was done simply by referring to "unperturbed" flux and fission-density distributions given in the Guide for Irradiation Experiments in EBR-II,[4] making simple corrections for the different nominal power levels at which the reactor has operated, and using a constant factor to convert total fission rate to power. A major difficulty is that the data in Ref. 4 (Table C-1) are intended only for use in scoping calculations in experimental design. Implicit in this approach are two assumptions--the nominal reactor power is the actual power, and the relative flux and power distributions are the same in the run or runs of interest as those calculated for the configurations used as a basis for Ref. 4. The first of these assumptions, related to the uncertainty in EBR-II total power from run to run, is not considered here.

The second assumption, concerning the relative flux and power distributions, has the following sources of error:

1. The "unperturbed" radial and axial flux and fission-rate distributions given in Ref. 4 are by definition based on neutronics calculations in cylindrical geometry in which: (a) the hexagonal-row structure is treated as a cylinder, and (b) the subassembly compositions must be homogenized by row and thus cannot really display either global-flux asymmetry or local perturbations.

2. As the reactor configuration changes from run to run, the spatially detailed distributions change.

3. The use of a constant factor to convert total fission rate to power is not rigorously correct.

The heterogeneous loadings in EBR-II lead to asymmetry and perturbation effects, as transport-theory calculations in X-Y geometry have shown.[4-6] Thus, the "unperturbed" distributions calculated for a specific heterogeneous EBR-II configuration are only approximate--i.e., their main value is in scoping calculations. To obtain spatially detailed distributions for a given configuration, neutronics calculations in hexagonal or X-Y geometry, as well as in R-Z geometry, are required. If an experiment is in EBR-II for several runs, more than one set of detailed distributions will usually be required to characterize the reactor environment during the irradiation interval of interest. The total rate of energy absorption at a point in the reactor has two components, one due to the kinetic energy of fission

fragments and β-particles, and the other due to deposition of γ energy. Fission-fragment and β-particle energy produced at a point is all absorbed at, or very close to, the point. Some of the γ energy produced as a result of fission, however, is absorbed at a distance from the point of fission. Therefore, the total rate of energy absorption at a point will have a distribution specific to a given reactor configuration and somewhat different from the fission-rate distribution for that configuration.

Ideally, then, a two-dimensional transport-theory calculation in hexagonal or X-Y geometry should be made for every run to obtain a detailed mapping of peak absolute fluxes and fission densities. Relative axial distributions should be obtained from transport calculations in R-Z geometry that are run less frequently. (Axial distributions in R-Z geometry change less from run to run than do X-Y distributions.) Corresponding γ-transport calculations should also be made. From this information, plus a knowledge of the duration of each startup and shutdown and of run length, the flux and power history of any element irradiated in EBR-II could be obtained in great detail. Techniques for computing a detailed three-dimensional mapping of absolute fluxes, fission rates, and γ-heating rates have been developed by the EBR-II Project. Techniques for computing the burnup of heavy atoms more precisely and for developing the history of individual elements irradiated in EBR-II are being developed.

However, X-Y neutron-transport calculations have been completed for only 31 of the approximately 200 run configurations. These calculations can be used to estimate the average flux and power distributions for given elements irradiated in EBR-II. The resulting averages account for most of the local and global variations in flux in the reactor during the irradiation period of interest; thus, the averages are a significant improvement over the use of information from only one run (such as that given in Ref. 4). An improved method for characterizing the average neutronic environment of oxide elements irradiated in EBR-II is described in this report.

Briefly, the total number of runs during which a given experimental subassembly is in EBR-II is subdivided into groups of runs. Runs with nearly the same neutronic characteristics are grouped. An X-Y transport-theory calculation on one representative configuration in each group gives peak absolute fluxes and fission densites (fission rate per gram of a heavy nuclide) at four points in every subassembly in the reactor. The distributions of fluxes and fission densities are used to estimate peak absolute fluxes and fission densities in each element in the subassembly of interest. Relative axial distributions are obtained from transport-theory calculations in R-Z geometry, which are run less frequently. Each absolute axial distribution is obtained from the peak absolute value from (a) the X-Y calculation and (b) the relative axial distribution calculated in R-Z geometry for the row in which the irradiation took place. The power in each of, for example, 20 axial nodes of an element is obtained by multiplying the average

fission rate per gram of each heavy nuclide--^{235}U, ^{238}U, ^{239}Pu, and ^{240}Pu--in the node by its midirradiation mass in the node and summing over the four heavy nuclides. Midirradiation masses are calculated from initial masses by correcting for burnup. The resulting distributions can then be used to represent the group of runs for the number of megawatt-days of irradiation involved, or, if desired, different groups can be averaged on a megawatt-day basis to estimate the overall average distributions for the irradiation of interest.

II. NEUTRONICS-CHARACTERIZATION METHOD

A. EBR-II Operating History

EBR-II has undergone many important changes since it was first operated at 45 MWt. These changes were in designs of the driver, safety, and control subassemblies, temporary replacement of some uranium radial-blanket subassemblies with stainless steel reflector subassemblies, run-to-run changes in configuration, and operation at different nominal total powers. The length of the metal fuel pin was reduced from 14.2 in. in the Mark-I element to 13.5 in. in the Mark-IA element to accommodate fuel swelling and decrease the plenum pressure. This change in the active core height of EBR-II took place gradually, as Mark-I elements were replaced by Mark-IA elements between runs 13 and 25, most of the change taking place between runs 15 and 19. Similarly, for economy, the upper and lower uranium axial-blanket elements used in driver, safety, and control subassemblies were replaced, between runs 14 and 25, with stainless steel trifluted sections. During runs 25-29A, the uranium radial-blanket subassemblies in rows 7 and 8 were replaced by stainless steel reflector subassemblies. This change significantly reduced the power coefficient of reactivity; the reduction was subsequently ascribed to anomalous bowing of subassemblies in row 8 induced by thermal gradients.[7] While this effect was being studied, the stainless steel reflector subassemblies in row 7 were replaced with uranium blanket subassemblies for run 29B. In run 29C, the same change was made in row 8. The reactor has been operated with such blanket subassemblies to date. The run-to-run changes in the configuration of EBR-II are shown in EBR-II run reports, which are compiled periodically.[8]

Up to and including run 29D, EBR-II was operated at a nominal total power of 45 MWt. From run 30A to run 37, it was operated at 50 MWt. During run 38A, it underwent trial operation at 62.5 MWt, and from run 38B to run 45B, it was again operated at 50 MWt. Since run 46A, EBR-II has been operated at a nominal total power of 62.5 MWt.

B. Neutronic Representations

A diagram of the EBR-II core cross section[9] (rows 1-7) is shown in Fig. 1. A two-dimensional transport-theory calculation for the plane of this

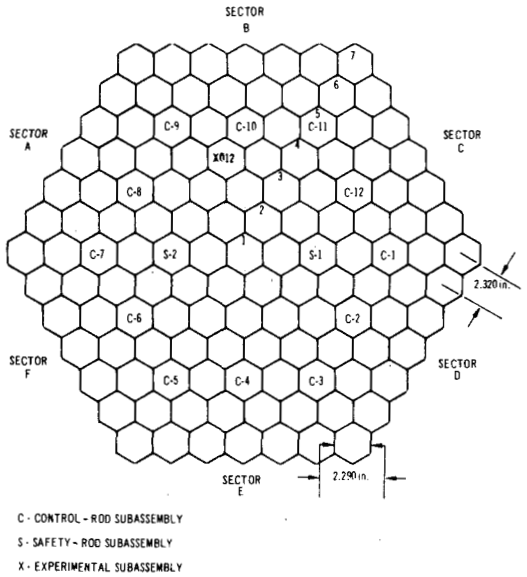

Fig. 1. EBR-II Core Configuration

cross section using a hexagonal coordinate system would be desirable, but an operational computer code with such a capability is not yet available to the EBR-II Project. As a close approximation, an X-Y coordinate system, shown in Fig. 2, is used for EBR-II transport-theory calculations with the DOT code.[5] Each hexagonal subassembly is represented by an equivalent rectangle, and each rectangle is subdivided into four elements of equal area for the calculations, as shown in Fig. 3. For a given reactor configuration, the X-Y transport-theory calculation gives peak absolute group fluxes and corresponding fission rates per atom of ^{235}U, ^{238}U, ^{239}Pu, and ^{240}Pu at each of the four points shown as crosses in Fig. 3, in

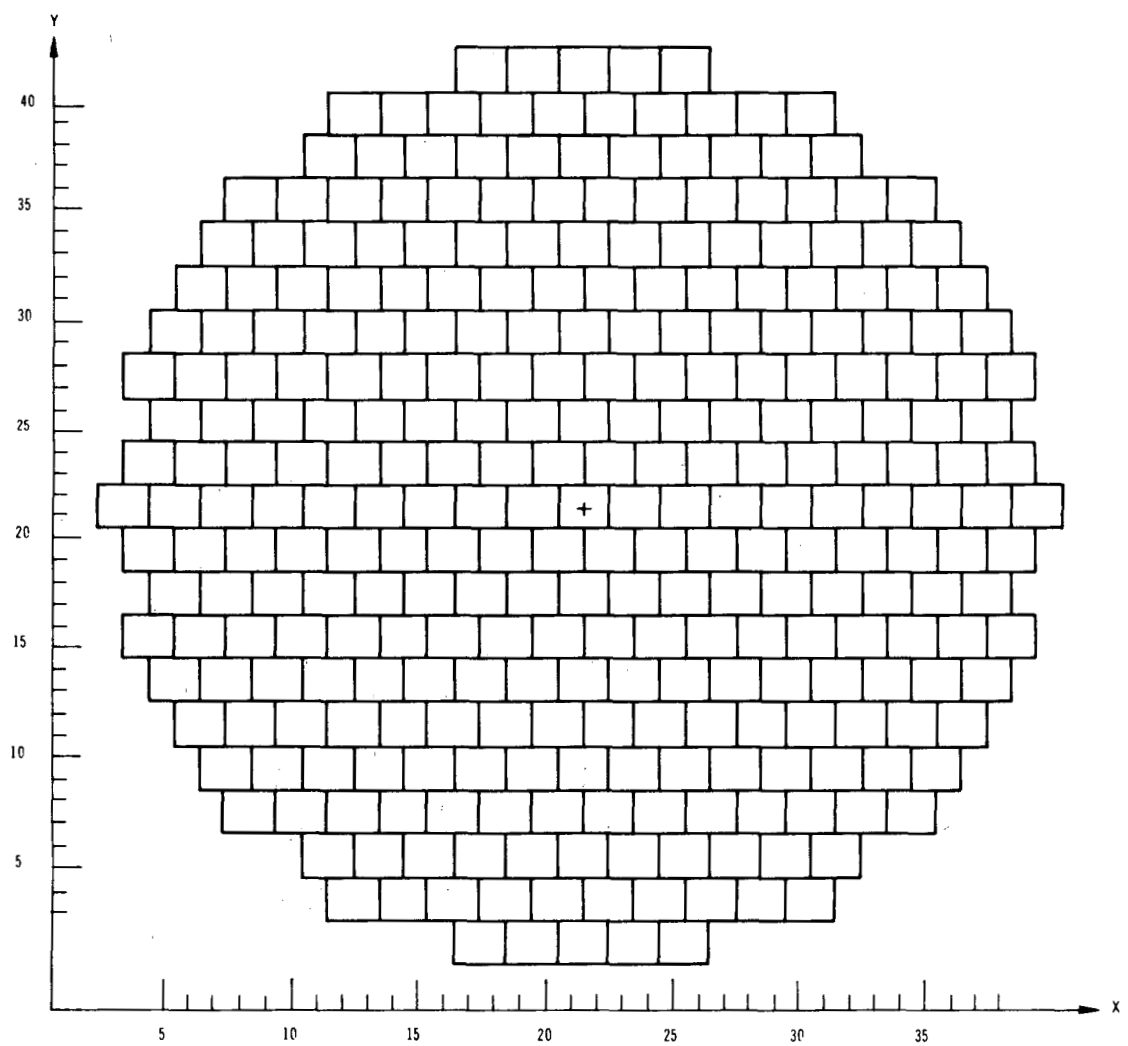

Fig. 2. X-Y Representation of EBR-II Cross Section

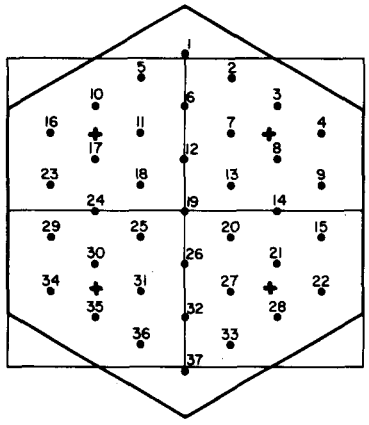

Fig. 3. Representation of EBR-II Spatial Hexagon in DOT X-Y Transport-theory Calculation

every subassembly in the reactor. Figure 3 also shows (as dots) the location of each element in an experimental 37-element subassembly. The specific location of each element in every experimental subassembly irradiated in EBR-II through run 42 is given in Ref. 10.

In the X-Y calculations, material compositions are homogenized for individual subassemblies. Transverse leakage is accounted for in the X-Y calculations by adding a fictitious absorption term $D_{sj}B_z^2$ to the absorption and total cross sections in each energy group j for each subassembly s. The diffusion coefficients, D_{sj}, most nearly correct for each subassembly in the reactor were selected from nine sets of values of D_j computed for nine typical subassemblies. (The Argonne version of the DOT code has recently been revised to compute the values of D_{sj} from the input transport cross sections and subassembly compositions.) One region-independent value of transverse buckling, B_z^2, was used for all EBR-II configurations in the present work. This value was originally determined by adjusting transverse leakage until corresponding X-Y and R-Z calculations on an earlier EBR-II configuration converged to the same eigenvalue. Similar calculations on a recent configuration have confirmed the original buckling value.

Some indication of the accuracy of the results is provided by comparing control-rod worths calculated by these methods with measured worths. Calculated and measured rod worths for EBR-II run 27A are plotted on polar coordinates in Fig. 4. The largest difference--4.2%--between the calculated and measured values occurs at control rod No. 7. Since the control-rod worth is approximately proportional to the square of the flux, the indicated maximum relative error in flux is about 2%. Figure 4 also shows a significant global variation in flux in run 27A.

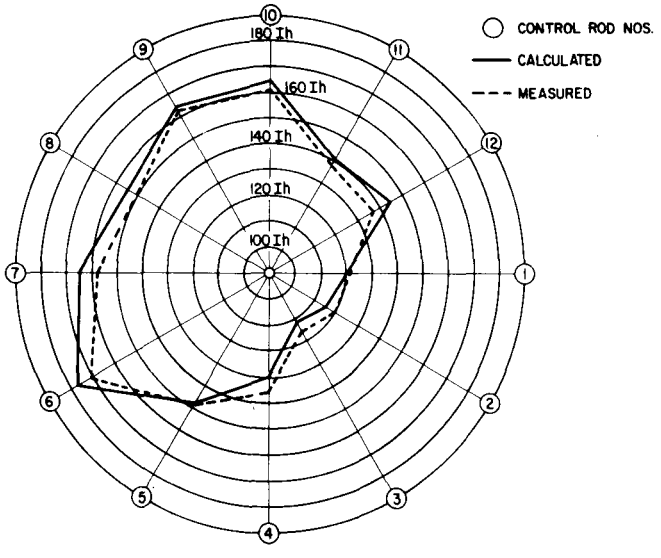

Fig. 4

Control-rod Worths for EBR-II Run 27A. ANL Neg. No. 104-344.

The relative axial distributions of flux and fission densities are obtained from transport calculations with the DOT code in R-Z geometry. As noted earlier, these distributions change less from run to run than do the X-Y distributions. This lesser variation is partly real, because changing one subassembly generally has little effect on axial flux and fission-density distributions several subassemblies away. There is, however, some artificiality because of the required homogenization by row of subassembly compositions. Thus, if one subassembly in one row is changed, its homogenized effect becomes progressively smaller with increasing row number, i.e., with increasing number of subassemblies in the row.

Over several runs, the relative axial distributions may vary enough so that some account of them must be taken. The axial distributions of group fluxes, total flux, and each of the fission densities for ^{235}U, ^{238}U, ^{239}Pu, and ^{240}Pu all differ at a given radial position in a given configuration. For the group flux distributions, this difference is due to the "softening" of the flux spectrum with increasing distance from the core center. For fission-density distributions, the difference is due to the flux softening and to the specific variation of each fission cross section with neutron energy. Hence, ^{238}U, which, for fission, has a relatively high threshold energy and a relatively low cross section, has a larger maximum-to-average axial distribution than ^{240}Pu, which fissions at lower energies and has a higher fission cross section.[11] Similarly, ^{235}U and ^{239}Pu have relatively flat axial fission-density distributions because their fission cross sections vary less through the neutron-energy range of interest for EBR-II. In the Guide for Irradiation Experiments in EBR-II,[4] the axial fission-density distributions for ^{235}U and ^{239}Pu are indicated as being the same. As will be shown, this assumption is only an approximation.

An R-Z calculation yields the fission rate in the three-dimensional reactor by assuming azimuthal symmetry and an arbitrary power level. The fission rate is integrated over the reactor volume, and the total power generated at the arbitrary level of the calculation is determined by using the value of 202.6 MeV/fission as the total energy deposited in the reactor per fission. This energy includes that produced by neutron capture and subsequent γ emission, and it excludes neutrino energy. The fission-rate distribution is then renormalized to correspond to the nominal total reactor power.

The correctly normalized fission rate is then integrated over a unit height at the reactor midplane. The fission-rate distribution as computed in the X-Y analysis is also integrated over a unit height at the reactor midplane and then renormalized so that the integral of the fission rate from the X-Y problem agrees with the integral of the fission rate over the reactor midplane of the correctly normalized R-Z fission distribution. The neutron fluxes and the fission rates of the individual isotopes are then normalized to correspond to the nominal reactor power by using the normalization factor

computed on the basis of the total fission rates. The X-Y normalization factor determined for a run that is analyzed in both R-Z and X-Y geometry is used to normalize X-Y problems for several subsequent runs.

C. Averaging Procedures

The total irradiation time of a given experiment is divided into groups of runs, in each of which absolute X-Y distributions, especially in the neighborhood of the experiment, remain essentially constant. This constancy is determined by noting variations in loadings and in measured control-rod worths from run to run. An X-Y transport calculation for one configuration in each group is used to represent the total megawatt-days of irradiation for the group. The resulting set of average X-Y distributions can be either used directly in fuel-lifetime calculations or averaged overall on a megawatt-day basis. This averaging is done by weighting the representative distributions for each group by the fraction of the total megawatt-days spent by the experiment in that group and summing over all groups. If the relative axial distributions vary sufficiently over the total irradiation time, axial distributions from several R-Z configurations are used. These distributions can be employed directly with individual representative X-Y distributions, or they can be grossly averaged on a megawatt-day basis to be used with the overall average X-Y distribution.

D. Treatment of Burnup

In the computation of the power generation in a fuel element, account should be taken of heavy-atom depletion due to burnup. Consider an element for which overall-average absolute peak fission densities and corresponding average relative axial distributions have been computed. To calculate the midlife power generation along this element, the axial distribution of heavy atoms at midlife is estimated. The equations used in this estimation are derived in Appendix A. Conversion of ^{238}U to ^{239}Pu and ^{239}Pu to ^{240}Pu must also be considered. This conversion is considered in the next section for experimental oxide element C17 in subassembly X012, which was irradiated to a computed burnup of 9.5%.

III. CHARACTERIZATION OF SUBASSEMBLIES

A. Subassembly X012

1. Irradiation History

At the start of run 21, experimental subassembly X012, containing 19 encapsulated oxide fuel elements, was placed in position 4B2 of EBR-II (see Fig. 1). Its subsequent history in the reactor is summarized in Table I. Also shown in the table are the six surrounding subassemblies

and the number of megawatt-days of irradiation for each run. The reactor underwent changes in configuration and nominal power during the time it contained subassembly X012. These changes are summarized in Table II, which shows four significantly different configurations and two different nominal powers during the period of interest. Hence, three different configurations were selected for operation at 45 MWt, and a fourth configuration was selected for operation at 50 MWt, as shown in Table II. Run 29B was placed in the third configuration (which included runs 29B-29D) rather than the second on the basis of its row-7 uranium blanket. Subassembly X012 was thus in configurations similar to that of run 24 for 2975 megawatt-days

Table I. History of Subassembly X012 in EBR-II Position 4B2 (Ref. 8)

Run	MWd	Surrounding Subassemblies[a]	Run	MWd	Surrounding Subassemblies[a]
21	610	5D, 1C	30B	166	3D, 1C, X027, X040
22	1045				
23	690		30C	52	
24	630		31A	89	
25A	641	4D, 1C, 1P	31B	159	
25B	150		31C	84	
25C	723		31D	372	
25D	34		31E	0	
25E	13		31F	413	
26A	87		31G	111	
26B	1029	5D, 1C	32A	852	
26C	619	4D, 1C, X027	32B	249	
27A	283		32C	72	
27B	177		32D	224	
27C	62		33A	600	
27D	286		33B	576	
28C	669		34A	822	
29A	188		34B	310	
29B	24		35	1202	2D, 1C, MK-II, X027, X040
29C	205				
29D	710		36A	800	3D, 1C, MK-II, X027
30A	652	3D, 1C, X027, X040	36B	400	
			37	1196	

[a]C = control; D = driver; MK-II = Mark-II driver; P = half driver fuel, half stainless steel.

TABLE II. Changes in Configuration and Power in EBR-II during Residence of Subassembly X012

	Nominal Power, MWt				
	45				50
Runs	4-24	25-29A	29B	29C, 29D	30A-37
Configuration	First	Second	Third		Fourth
Description	Depleted-uranium blanket; for rows 15-19, core height reduced from 14.22 to 13.5 in.	SS in rows 7, 8	Uranium in row 7; SS in row 8	Depleted-uranium blanket	Depleted-uranium blanket
MWd	2975	4961	939		9401
Represented by Run	24	27A	29D		31F

or 0.1628 of its total of 18,276 megawatt-days of irradiation. The corresponding residence fractions for runs similar to 27A, 29D, and 31F are 0.2714, 0.0514, and 0.5144, respectively. By using the total megawatt-days and nominal powers for each configuration in Eq. A.1 (in Appendix A), the total irradiation time of X012 was calculated to be 3.329×10^7 sec.

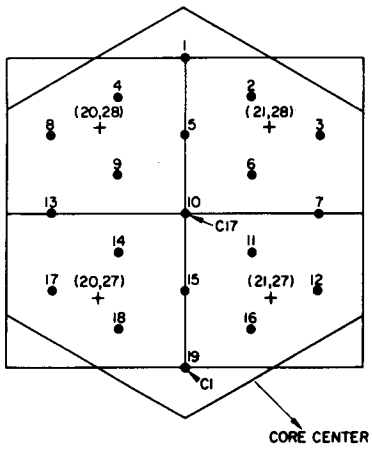

Fig. 5. X-Y Representation of Subassembly X012

2. X-Y Transport-theory Calculations

The X-Y transport-theory calculations were done in the S_2 approximation with the six-group ANL-23806 cross-section set.[12] Peak absolute fluxes and fission rates per atom were obtained for the four points identified with (X,Y) coordinates in Fig. 5. Table III gives results of the calculations for the representative runs 24, 27A, 29D, and 31F. In Table III, E_L represents lower energy limits in the six-group cross-section set used. The fluxes and fission rates per atom for run 27A are about 10% higher than corresponding values for runs 24 and 29D, largely owing to the replacement of fissionable blanket material by nonfissionable reflector material, which requires more power to be generated in the core for the fixed total power of 45 MWt.

TABLE III. Peak Absolute Fluxes and Fission Rates for Subassembly X012 in Runs 24, 27A, 29D, and 31F

Run (nominal power, MWt)	Position (X,Y)[a]	Midplane Flux in Group x 10^{-14}						$\sum \phi_j \times 10^{-15}$	Fission Rates ($\Sigma\sigma_{fj}\phi_j$) x 10^9			
		Group 1: E_L = 2.23 MeV	Group 2: E_L = 821 keV	Group 3: E_L = 302 keV	Group 4: E_L = 111 keV	Group 5: E_L = 40.9 keV	Group 6: E_L = 29 eV		^{235}U	^{238}U	^{239}Pu	^{240}Pu
24 (45); Uranium blanket	20,28	1.721	4.310	6.606	4.906	1.961	0.6620	2.017	2.816	0.1850	3.354	1.325
	21,28	1.750	4.388	6.710	4.965	1.980	0.6666	2.046	2.855	0.1883	3.403	1.347
	21,27	1.919	4.772	7.198	5.239	2.057	0.6779	2.186	3.041	0.2056	3.640	1.461
	20,27	1.822	4.606	7.052	5.174	2.041	0.6788	2.137	2.978	0.1967	3.555	1.412
27A (45); SS in rows 7, 8	20,28	1.995	4.945	7.405	5.344	2.084	0.7344	2.251	3.134	0.2135	3.751	1.511
	21,28	1.871	4.808	7.364	5.369	2.110	0.7693	2.229	3.114	0.2035	3.709	1.468
	21,27	2.054	5.194	7.825	5.633	2.189	0.7698	2.366	3.295	0.2218	3.942	1.583
	20,27	2.065	5.196	7.813	5.605	2.172	0.7490	2.360	3.282	0.2225	3.932	1.584
29D (45); Uranium blanket	20,28	1.729	4.391	6.668	4.955	1.989	0.6838	2.042	2.853	0.1871	3.396	1.343
	21,28	1.624	4.277	6.638	4.992	2.017	0.7149	2.026	2.841	0.1786	3.365	1.307
	21,27	1.798	4.639	7.058	5.215	2.079	0.7213	2.151	3.005	0.1959	3.578	1.414
	20,27	1.772	4.580	7.020	5.184	2.064	0.7018	2.132	2.977	0.1932	3.545	1.398
31F (50); Uranium blanket	20,28	1.960	4.872	7.201	5.484	2.220	0.7841	2.252	3.155	0.2100	3.749	1.487
	21,28	1.760	4.628	7.137	5.517	2.259	0.8237	2.212	3.114	0.1935	3.673	1.414
	21,27	1.932	5.034	7.633	5.754	2.323	0.8227	2.350	3.293	0.2115	3.907	1.532
	20,27	2.051	5.189	7.697	5.709	2.282	0.7796	2.370	3.309	0.2215	3.947	1.577

[a]See Figs. 2 and 5.

The ratio of fission rates per atom,

$$\sum_J \sigma_{fj}^{238}\varphi_j \Big/ \sum_J \sigma_{fj}^{235}\varphi_j,$$

increases with increasing hardness of the spectrum. At position (21,28), the ratio is 0.066 in run 24 and 0.062 in run 31F. The somewhat softer spectrum in run 31F is due to two adjacent experimental subassemblies containing oxide fuel.

Table C-1 of Ref. 4 gives unperturbed fission rates at the center of the 4B2 position of the run 29D configuration for a nominal reactor power of 62.5 MWt (i.e., the hexagonal row structure is treated as a cylinder, and fission rates are averaged by row). These fission rates can be compared with average values computed from the data of Table III for run 29D. For ^{235}U, Table III gives

$$\tfrac{1}{4}(2.853+2.841+3.005+2.977) \times 10^{-9} \times 6.0225 \times 10^{23}/235.04 =$$

$$0.748 \times 10^{13} \text{ fissions/g-sec}$$

at 45 MWt. The corresponding fission density from Table C-1 of Ref. 4, normalized to 45 MWt reactor power, is 0.697×10^{13} fissions/g-sec; the difference is 6.8%. Similarly, for ^{238}U the average from Table III is 0.477×10^{12}; the value from Ref. 4 is 0.452×10^{12} fissions/g-sec. Here the difference is 5.2%. Measured control-rod worths confirm that the flux tended to peak in the B sector of the core during run 29D.

3. Relative Axial Distributions

As mentioned earlier, axial distributions of flux and fission densities vary little from run to run. However, a major change in configuration, such as the introduction of two rows of stainless steel reflector subassemblies at the core edge (see Table II), would be expected to affect axial distributions significantly. Three representative R-Z configurations were thus selected to estimate average axial distributions for subassembly X012--runs 24, 27A, and 31F. For runs 24 and 27A, S_2 transport calculations were done with the six-group ANL-23806 cross-section set, and for run 31F with the 22-group ANL-238 set.[12] For X012, the axial distributions were all determined at a radius, r, of 14.92 cm from the central axis of the core (the center of position 4B2 corresponds to r = 15.59 cm). Since axial distributions have been found to vary little over the first five rows of EBR-II with a six-row core, the resulting distributions were assumed constant over the 4B2 position.

Figure 6 shows the relative distribution of total flux between the bottom and top of the core for runs 24, 27A, and 31F. The distribution for run 27A differs appreciably from the distributions for runs 24 and 31F. At each axial position, the total flux for each configuration was weighted according to the fraction of the total megawatt-days spent in similar configurations. The weight factors used were:

Run 24: $2975/18276 = 0.1628$

Run 27A: $4961/18276 = 0.2714$

Run 31F: $(939+9401)/18276 = 0.5658$

The resulting average curve is shown in Fig. 6.

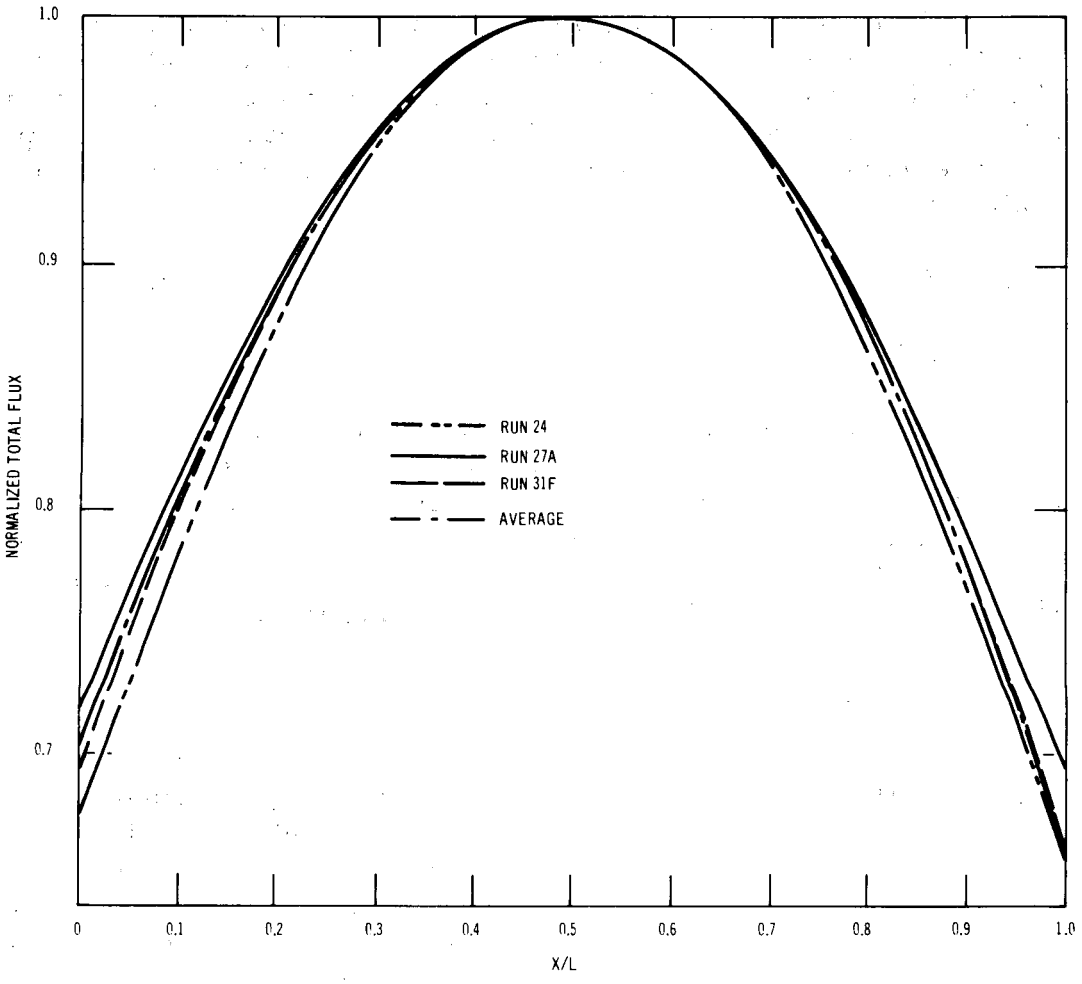

Fig. 6. Axial Distribution of Total Flux for Runs 24, 27A, and 31F

The axial profiles of fission density for ^{235}U, ^{238}U, ^{239}Pu, and ^{240}Pu were estimated in a similar manner, as shown in Figs. 7-10. The resulting averaged distributions were used to estimate the average relative flux and fission densities in each of 20 axial nodes, as shown in Table IV. Note in this table the differences between the distributions.

4. Element C17

Encapsulated element C17 was at the center of subassembly X012 (see Fig. 5). Hence the peak total flux in C17, in each of the four representative configurations, was taken as the average of the four values given in column 9 of Table III. Each resulting average was then weighted according to the fraction of the total megawatt-days associated with the configuration, e.g., a residence fraction of 0.1628 for the run-24 configuration (see Sec. III.A.1 above). The sum of the weighted averages was the average peak flux for C17: 2.254×10^{15} neutrons/cm^2-sec. The average peak fission densities for ^{235}U, ^{238}U, ^{239}Pu, and ^{240}Pu were estimated in the same way to be 0.8074×10^{13}, 0.5244×10^{12}, 0.9451×10^{13}, and 0.3728×10^{13} fissions/g-sec, respectively.

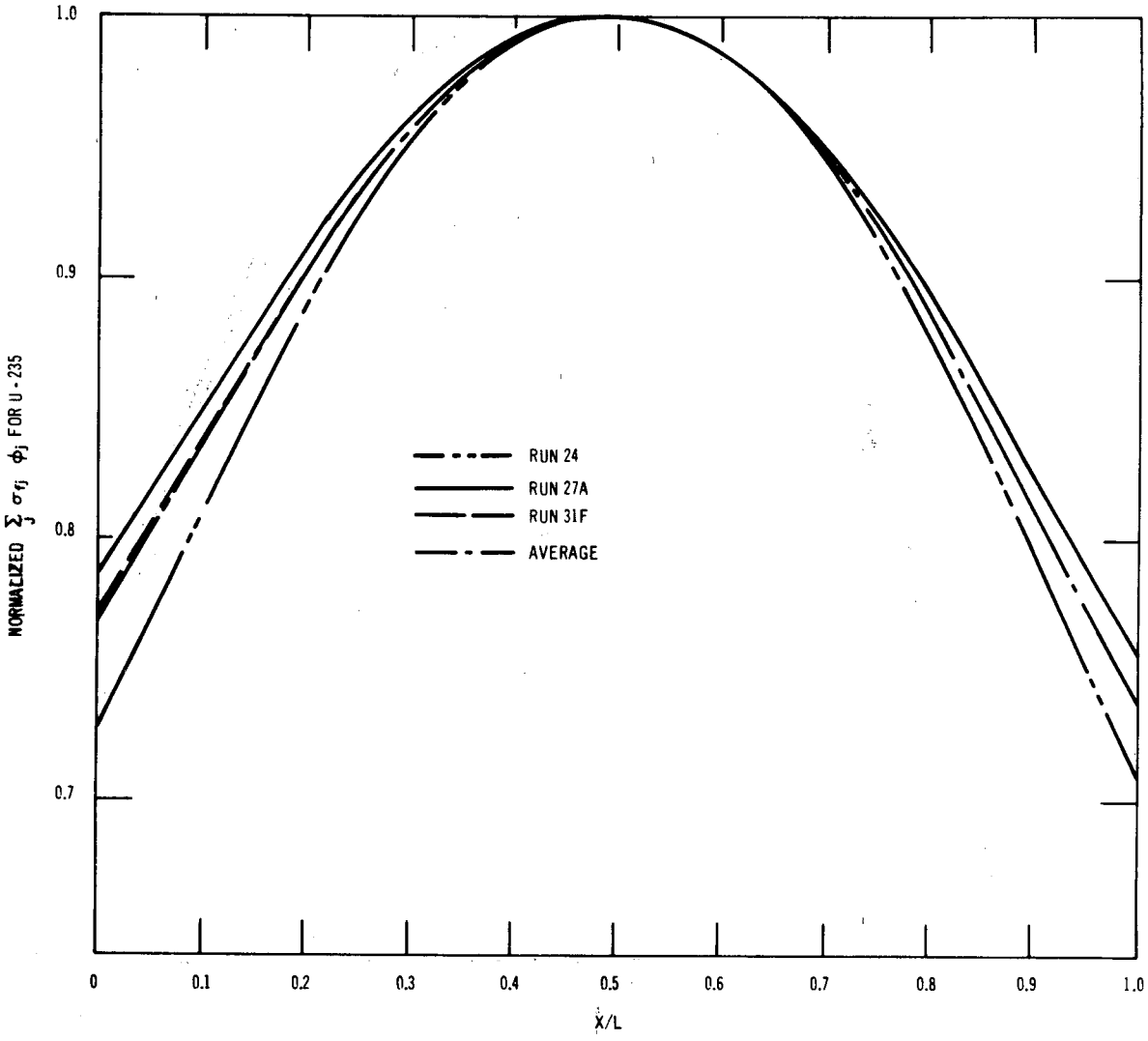

Fig. 7. Axial Distribution of ^{235}U Fission Density for Runs 24, 27A, and 31F

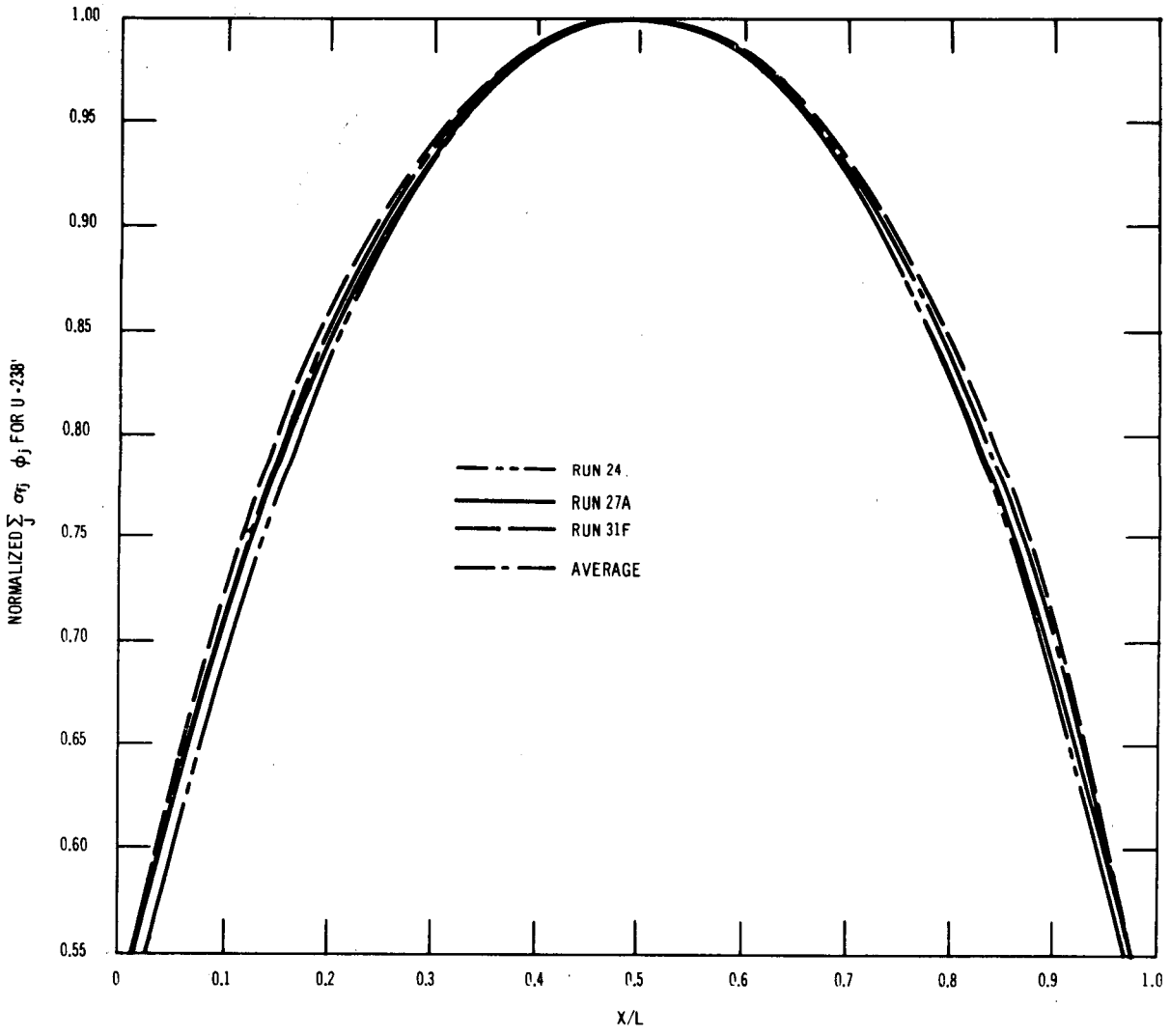

Fig. 8. Axial Distribution of ^{238}U Fission Density for Runs 24, 27A, and 31F

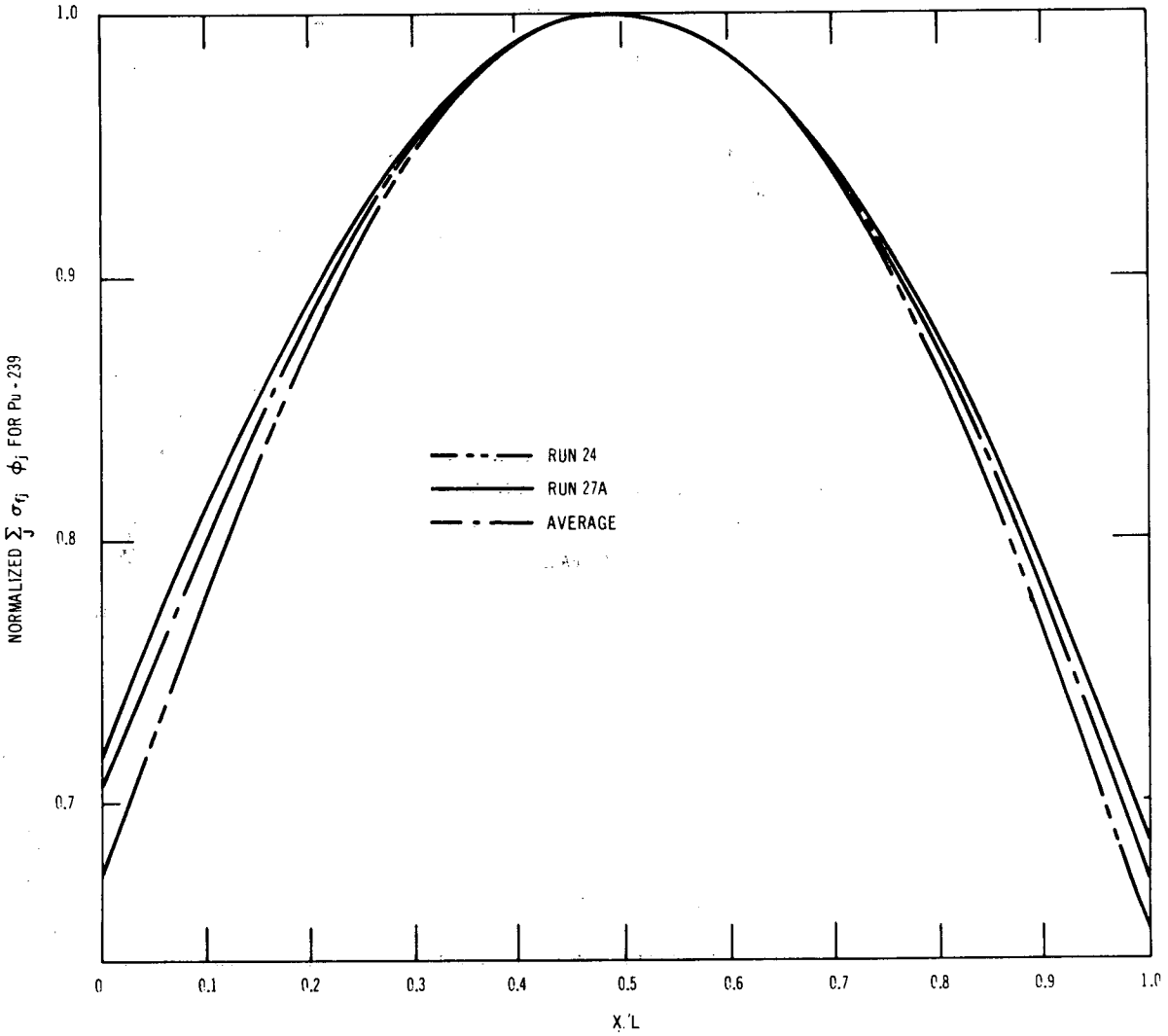

Fig. 9. Axial Distribution of ^{239}Pu Fission Density for Runs 24 and 27A

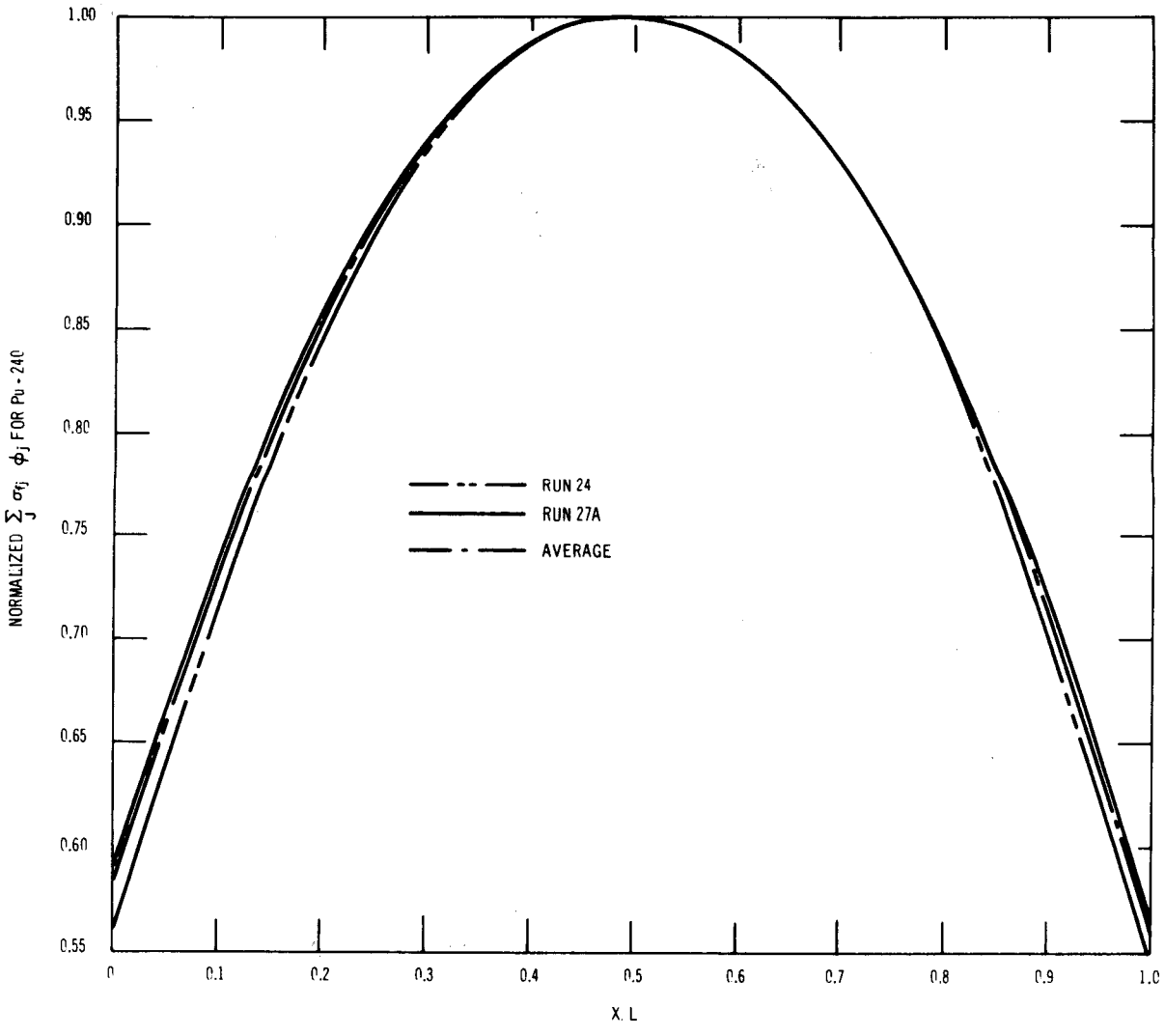

Fig. 10. Axial Distribution of ^{240}Pu Fission Density for Runs 24 and 27A

TABLE IV. Axial Distributions of Total Flux and Fission Density for Position 4B2, Averaged over Runs 21-37

Axial Position above Core Bottom	$\frac{\sum_J \varphi_j(k)}{\sum_J \varphi_{j,max}}$ [a]	$\frac{\sum_J \sigma_{fj}^{235}\varphi_j(k)}{\sum_J \sigma_{fj}^{235}\varphi_{j,max}}$	$\frac{\sum_J \sigma_{fj}^{238}\varphi_j(k)}{\sum_J \sigma_{fj}^{238}\varphi_{j,max}}$	$\frac{\sum_J \sigma_{fj}^{239}\varphi_j(k)}{\sum_J \sigma_{fj}^{239}\varphi_{j,max}}$	$\frac{\sum_J \sigma_{fj}^{240}\varphi_j(k)}{\sum_J \sigma_{fj}^{240}\varphi_{j,max}}$
k = 1	0.7280	0.7859	0.559	0.730	0.625
2	0.7746	0.8195	0.661	0.777	0.699
3	0.8210	0.8529	0.752	0.822	0.769
4	0.8678	0.8861	0.823	0.865	0.830
5	0.9068	0.9185	0.877	0.904	0.879
6	0.9380	0.9459	0.920	0.936	0.921
7	0.9642	0.9683	0.954	0.962	0.954
8	0.9827	0.9849	0.979	0.983	0.978
9	0.9943	0.9960	0.994	0.995	0.993
10	1.000	1.000	1.000	1.000	1.000
11	0.9985	0.9993	0.999	0.999	1.000
12	0.9908	0.9922	0.990	0.991	0.991
13	0.9771	0.9793	0.972	0.978	0.973
14	0.9550	0.9588	0.946	0.955	0.946
15	0.9260	0.9342	0.911	0.926	0.910
16	0.8913	0.9047	0.867	0.891	0.868
17	0.8523	0.8692	0.811	0.851	0.816
18	0.8057	0.8318	0.738	0.802	0.757
19	0.7530	0.7947	0.648	0.751	0.684
20	0.6966	0.7570	0.558	0.701	0.606

[a] $\varphi_{j,max} \equiv \varphi_j(10)$.

The average total flux in each of the 20 axial nodes was taken as the product of the average peak flux for C17 and the relative axial-flux factor given in column 2 of Table IV. The resulting distribution is shown in column 2 of Table V. The axial distributions of fission rate per gram of ^{235}U, ^{238}U, ^{239}Pu, and ^{240}Pu, which were computed in a similar manner, are given in columns 5, 9, 13, and 17, respectively, of Table V.

The initial mass distributions of the heavy isotopes in subassembly C17 (Ref. 13) are shown in columns 3, 7, 11, and 15 of Table V. To compute the average (midlife) power generation in C17, these distributions were corrected for burnup by using the technique given in Appendix A. This technique gave the following peak burnups in atom of isotope per initial atom:

^{235}U: 0.0997;

^{238}U: 0.0069;

^{239}Pu: 0.1175;

^{240}Pu: 0.0490.

In the power-distribution calculations, burnup of ^{238}U was neglected because it was less than 1%, and burnup of ^{240}Pu was neglected because of its low initial concentration. By use of the above individual burnup values in Eq. A.7, the total peak burnup in C17 was calculated to be 9.6%.

TABLE V. Axial Distributions of Total Flux and Power in Element C17 in Subassembly X012

Axial Node	$\phi_{total} \times 10^{-15}$	^{235}U Weight, g At t = 0	^{235}U Weight, g At Midlife	^{235}U $\frac{N_0}{A}\sum_J \sigma_{fj}\phi_j$, fiss/sec-g x 10^{-13}	^{235}U Midlife Fission Rate, fiss/sec x 10^{-13}	^{238}U Weight, g At t = 0	^{238}U Weight, g At Midlife	^{238}U $\frac{N_0}{A}\sum_J \sigma_{fj}\phi_j$, fiss/sec-g x 10^{-12}	^{238}U Midlife Fission Rate, fiss/sec x 10^{-13}	^{239}Pu Weight, g At t = 0	^{239}Pu Weight, g At Midlife	^{239}Pu $\frac{N_0}{A}\sum_J \sigma_{fj}\phi_j$, fiss/sec-g x 10^{-13}	^{239}Pu Midlife Fission Rate, fiss/sec x 10^{-13}	^{240}Pu Weight, g At t = 0	^{240}Pu Weight, g At Midlife	^{240}Pu $\frac{N_0}{A}\sum_J \sigma_{fj}\phi_j$, fiss/sec-g x 10^{-13}	^{240}Pu Midlife Fission Rate, fiss/sec x 10^{-13}	Total Fission Rate, fiss/sec x 10^{-13}	Power,[a] Btu/hr
1[b]	1.641	2.5985	2.4967	0.6346	1.5844	0.2539	0.2539	0.293	0.00744	0.6873	0.6578	0.690	0.4539	0.0447	0.0447	0.234	0.0105	2.0562	2145
2	1.746	2.5985	2.4924	0.6617	1.6492	0.2539	0.2539	0.347	0.00881	0.6873	0.6559	0.734	0.4815	0.0447	0.0447	0.261	0.0117	2.1512	2244
3	1.851	2.5985	2.4880	0.6887	1.7135	0.2539	0.2539	0.394	0.01000	0.6873	0.6541	0.777	0.5082	0.0447	0.0447	0.287	0.0128	2.2445	2342
4	1.956	2.5985	2.4837	0.7155	1.7771	0.2539	0.2539	0.432	0.01097	0.6873	0.6523	0.818	0.5336	0.0447	0.0447	0.309	0.0138	2.3355	2437
5	2.044	2.5985	2.4795	0.7416	1.8388	0.2539	0.2539	0.460	0.01168	0.6873	0.6508	0.854	0.5558	0.0447	0.0447	0.328	0.0147	2.4210	2526
6	2.115	2.5985	2.4760	0.7638	1.8912	0.2539	0.2539	0.482	0.01224	0.6873	0.6495	0.885	0.5748	0.0447	0.0447	0.344	0.0154	2.4936	2601
7	2.174	2.5985	2.4731	0.7818	1.9335	0.2539	0.2539	0.500	0.01270	0.6873	0.6485	0.909	0.5894	0.0447	0.0447	0.356	0.0159	2.5515	2662
8	2.215	2.5985	2.4709	0.7953	1.9651	0.2539	0.2539	0.513	0.01303	0.6873	0.6476	0.929	0.6016	0.0447	0.0447	0.365	0.0163	2.5960	2708
9	2.242	2.5985	2.4695	0.8042	1.9860	0.2539	0.2539	0.521	0.01323	0.6873	0.6471	0.940	0.6083	0.0447	0.0447	0.370	0.0165	2.6240	2738
10	2.254	2.5985	2.4690	0.8074	1.9936	0.2539	0.2539	0.5244	0.01331	0.6873	0.6469	0.9451	0.6114	0.0447	0.0447	0.3728	0.0167	2.6350	2749
11	2.251	2.5985	2.4691	0.8069	1.9923	0.2539	0.2539	0.524	0.01330	0.6873	0.6470	0.944	0.6107	0.0447	0.0447	0.372	0.0166	2.6329	2747
12	2.234	2.6075	2.4786	0.8011	1.9856	0.2505	0.2505	0.519	0.01300	0.6809	0.6412	0.937	0.6008	0.0443	0.0443	0.369	0.0163	2.6157	2729
13	2.203	2.6426	2.5136	0.7907	1.9875	0.2373	0.2373	0.510	0.01210	0.6559	0.6182	0.924	0.5712	0.0426	0.0426	0.363	0.0155	2.5863	2698
14	2.153	2.6426	2.5163	0.7742	1.9481	0.2373	0.2373	0.496	0.01177	0.6559	0.6191	0.903	0.5590	0.0426	0.0426	0.353	0.0150	2.5339	2644
15	2.088	2.6426	2.5195	0.7543	1.9005	0.2373	0.2373	0.478	0.01134	0.6559	0.6202	0.875	0.5427	0.0426	0.0426	0.339	0.0144	2.4689	2576
16	2.009	2.6426	2.5234	0.7305	1.8433	0.2373	0.2373	0.455	0.01080	0.6559	0.6216	0.842	0.5234	0.0426	0.0426	0.323	0.0138	2.3913	2495
17	1.921	2.6426	2.5281	0.7018	1.7742	0.2373	0.2373	0.425	0.01009	0.6559	0.6231	0.804	0.5010	0.0426	0.0426	0.304	0.0130	2.2983	2398
18	1.816	2.6426	2.5330	0.6716	1.7012	0.2373	0.2373	0.387	0.00918	0.6559	0.6250	0.758	0.4737	0.0426	0.0426	0.282	0.0120	2.1961	2291
19	1.698	2.6426	2.5379	0.6417	1.6286	0.2373	0.2373	0.340	0.00807	0.6559	0.6269	0.710	0.4451	0.0426	0.0426	0.255	0.0109	2.0927	2183
20	1.570	2.6426	2.5429	0.6112	1.5542	0.2373	0.2373	0.293	0.00695	0.6559	0.6289	0.663	0.4169	0.0426	0.0426	0.226	0.0096	1.9877	2074

[a]Based upon 190.8 MeV/fission.
[b]Bottom of core.

Although only 0.69% of the ^{238}U fissioned, its conversion to ^{239}Pu also had to be considered. For the run 29D configuration, the capture-to-fission ratio for ^{238}U,

$$\sum_J \sigma_{cj}^{238}\varphi_j(10) \Big/ \sum_J \sigma_{fj}^{238}\varphi_j(10),$$

was calculated to be 1.89 at the center of subassembly X012. Thus, only about 0.69 x 1.9 = 1.3% of the ^{238}U was converted to ^{239}Pu at axial node 10; this effect was neglected. The capture-to-fission ratio for ^{239}Pu was about 0.08 at axial node 10 in row 4. The conversion of ^{239}Pu to ^{240}Pu at this position was about 11.75 x 0.08 = 0.94% and thus was neglected. Therefore, in the power calculations, account was taken of only burnup of ^{235}U and ^{239}Pu.

Resulting midlife mass distributions are given in columns 4, 8, 12, and 16 of Table V; these data were used to compute the midlife fission rates, in columns 6, 10, 14, and 18, and the total fission rate, in column 19. In Appendix B, the effective MeV/fission is shown to be nearly constant over the length of element C17. Therefore, for simplicity the total fission rate in each axial node of C17 was converted to Btu/hr of power generation by using 190.8 MeV/fission. Results are given in the last column of Table V.

5. Element C1

The capsule containing element C1 is in the position in subassembly X012 shown in Fig. 5. This position was very nearly the same distance from the core center as the X-Y point (21,27). Hence, the peak flux and fission densities in C1 were taken as being equal to the values at (21,27) for each representative configuration. The same representative configurations, megawatt-day averaging, and relative axial distributions were used here as were used for element C17. Results of the calculations for element C1 are summarized in Table VI.

TABLE VI. Axial Distributions of Total Flux and Power in Element C1 in Subassembly X012

Axial Node	ϕ_{total} x 10^{-15}	Total Fission Rate, fissions/sec x 10^{-13}	Power,[a] Btu/hr	Axial Node	ϕ_{total} x 10^{-15}	Total Fission Rate, fissions/sec x 10^{-13}	Power,[a] Btu/hr
k = 1[b]	1.687	2.0778	2168	k = 11[b]	2.314	2.6164	2730
2	1.795	2.1640	2258	12	2.296	2.6251	2739
3	1.903	2.2490	2346	13	2.264	2.6677	2783
4	2.011	2.3332	2434	14	2.213	2.6135	2727
5	2.102	2.4144	2519	15	2.146	2.5471	2657
6	2.174	2.4833	2591	16	2.066	2.4667	2573
7	2.235	2.5393	2649	17	1.975	2.3708	2473
8	2.277	2.5804	2692	18	1.867	2.2651	2363
9	2.304	2.6080	2721	19	1.745	2.1581	2251
10	2.318	2.6180	2731	20	1.614	2.0497	2138

[a]Based upon 190.8 MeV/fission.
[b]Bottom of core.

B. Subassembly X012A

1. Irradiation History

Subassembly X012A was removed from EBR-II at the end of run 37 for interim examination. After the examination, all 19 encapsulated oxide elements originally in X012 were placed in their original position in a new subassembly, which was designated X012A. This subassembly was put back into position 4B2 of EBR-II at the start of run 39A; it remained there until it was removed from the reactor at the end of run 40B. The history of X012A in EBR-II is summarized in Table VII. The runs chosen for the representative X-Y configurations for this history are shown in Table VIII. The megawatt-day residence fractions for runs 24, 27A, 29D, 31F, and 39A were 0.1416, 0.2361, 0.0446, 0.4474, and 0.1313, respectively.

TABLE VII. History of Subassembly X012A in EBR-II Position 4B2 (Ref. 8)

Run	MWd	Surrounding Subassemblies[a]	Run	MWd	Surrounding Subassemblies[a]	Run	MWd	Surrounding Subassemblies[a]
21	610	5D, 1C	29D	710	4D, 1C, X027	35	1202	2D, 1C, MK-II, X027, X040
22	1045		30A	652	3D, 1C, X027, X040			
23	690					36A	800	3D, 1C, MK-II, X027
24	630		30B	166				
25A	641	4D, 1C, 1P	30C	52		36B	400	
25B	150		31A	89		37	1196	
25C	723		31B	159		39A	771	2D, 1C, X040A, X027, MK-II
25D	34		31C	84				
25E	13		31D	372		39B	185	1D, 1C, 70%, X027, MK-II, Test Leak
26A	87		31E	0				
26B	1029	5D, 1C	31F	413				
26C	619	4D, 1C, X027	31G	111		39C	415	2D, 1C, 70%, X027, MK-II
27A	283		32A	852				
27B	177		32B	249		40A	443	2D, 1C, X040A, X027, MK-II
27C	62		32C	72				
27D	286		32D	224		40B	924	2D, 1C, X040A, X027, MK-II
28C	669		33A	600				
29A	188		33B	576				
29B	24		34A	822				
29C	205		34B	310				

[a] C = control; D = driver; MK-II = Mark-II driver; P = half driver fuel, half stainless steel; 70% = 70% enriched driver fuel.

TABLE VIII. Changes in Configuration and Power in EBR-II during Residence of Subassembly X012A

	Nominal Power, MWt					
	45				50	
Runs	4-24	25-29A	29B	29C, 29D	30A-37A	39A-40B
Configuration	First	Second	Third		Fourth	Fifth
Description	Depleted-uranium blanket	SS in rows 7, 8	U in row 7; SS in row 8	Depleted-uranium blanket	Depleted-uranium blanket	Depleted-uranium blanket
MWd	2975	4961	939		9401	2738
Represented by run	24	27A	29D		31F	39A

2. Transport-theory Calculations

The X-Y transport-theory results for the 4B2 position of EBR-II for runs 24, 27A, 29D, and 31F are given in Table III; the results for run 39A are given in Table IX. The relative axial distributions used for subassembly X012A were the same as those used for subassembly X012, as shown in Table IV.

TABLE IX. Peak Absolute Fluxes and Fission Rates for Subassembly X012A in Run 39A[a]

Position (X,Y)	Midplane Flux in Group x 10^{-14}							Fission Rates ($\Sigma\sigma_{fj}\phi_j$) x 10^9			
	Group 1: E_L = 2.23 MeV	Group 2: E_L = 821 keV	Group 3: E_L = 302 keV	Group 4: E_L = 111 keV	Group 5: E_L = 40.9 keV	Group 6: E_L = 29 eV	$\sum \phi_j$ x 10^{-15}	^{235}U	^{238}U	^{239}Pu	^{240}Pu
20,28	2.053	5.070	7.445	5.698	2.340	0.854	2.346	3.295	0.2193	3.907	1.548
21,28	1.908	4.898	7.390	5.724	2.367	0.885	2.317	3.265	0.2075	3.815	1.496
21,27	2.066	5.251	7.834	5.974	2.440	0.890	2.446	3.434	0.2236	4.069	1.600
20,27	2.127	5.327	7.881	5.928	2.412	0.857	2.453	3.436	0.2287	4.085	1.623

[a]Nominal power 50 MWt; uranium blanket.

3. Elements C17 and C1

Since all the elements were in the same positions in subassembly X012A as in X012, the same procedures were used to calculate the axial distributions of power in C17 and C1 as were used for their residence in X012. Again, total fission densities were converted to power on the basis of 190.8 MeV/fission. Results are given in Tables X and XI.

TABLE X. Axial Distributions of Total Flux and Power in Element C17 in Subassembly X012A

Axial Node	ϕ_{total} x 10^{-15}	Total Fission Rate, fissions/sec x 10^{-13}	Power,[a] Btu/hr	Axial Node	ϕ_{total} x 10^{-15}	Total Fission Rate, fissions/sec x 10^{-13}	Power,[a] Btu/hr
k = 1[b]	1.654	2.0611	2150	k = 11[b]	2.269	2.6347	2749
2	1.760	2.1561	2249	12	2.251	2.6175	2731
3	1.865	2.2485	2346	13	2.220	2.5887	2701
4	1.972	2.3389	2440	14	2.170	2.5361	2646
5	2.060	2.4245	2529	15	2.104	2.4721	2579
6	2.131	2.4959	2604	16	2.025	2.3946	2498
7	2.191	2.5539	2664	17	1.937	2.3024	2402
8	2.233	2.5978	2710	18	1.831	2.2008	2296
9	2.259	2.6260	2740	19	1.711	2.0975	2188
10	2.272	2.6365	2751	20	1.583	1.9930	2079

[a]Based upon 190.8 MeV/fission.
[b]Bottom of core.

TABLE XI. Axial Distributions of Total Flux and Power in Element C1 in Subassembly X012A

Axial Node	ϕ_{total} x 10^{-15}	Total Fission Rate, fissions/sec x 10^{-13}	Power,[a] Btu/hr	Axial Node	ϕ_{total} x 10^{-15}	Total Fission Rate, fissions/sec x 10^{-13}	Power,[a] Btu/hr
k = 1[b]	1.699	2.0819	2172	k = 11[b]	2.331	2.6168	2730
2	1.808	2.1676	2261	12	2.313	2.6254	2739
3	1.916	2.2522	2350	13	2.281	2.6677	2783
4	2.026	2.3358	2437	14	2.229	2.6137	2727
5	2.117	2.4168	2521	15	2.161	2.5476	2658
6	2.189	2.4849	2592	16	2.080	2.4679	2575
7	2.251	2.5403	2650	17	1.989	2.3731	2476
8	2.294	2.5814	2693	18	1.881	2.2680	2366
9	2.321	2.6089	2722	19	1.758	2.1615	2255
10	2.334	2.6186	2732	20	1.626	2.0535	2142

[a]Based upon 190.8 MeV/fission.
[b]Bottom of core.

C. Subassembly X040A

1. Irradiation History

The irradiation history of subassembly X040A in EBR-II is shown in Table XII. Subassembly X040A was a 37-oxide-element subassembly, originally loaded into position 5B2 as X040 just before run 30A. It remained in position 5B2 through run 35, after which it was removed for interim examination. All its elements except one were then put in a new subassembly can in their original positions. The exception, element 012 in position 22 (see Fig. 3), was replaced by a stainless steel dummy element. The subassembly, designated as X040A, was put back in position 5B2 just before run 38B. During runs 39B and 39C, this subassembly was in the 5B4 position. It was returned to the 5B2 position for run 40A and remained there until the end of run 42A, when it was removed from the reactor.

TABLE XII. History of X040A in EBR-II Positions 5B2 and 5B4

Run	MWd	Surrounding Subassemblies[a]	Run	MWd	Surrounding Subassemblies[a]
30A	652	D, D, C10, C9, D, X012	33B	576	D, D, C10, C9, D, X012
30B	166	D, D, C10, C9, 70%, X012	34A	822	D, D, C10, C9, 70%, X012
30C	52	D, D, C10, C9, D, X012	34B	310	D, D, C10, C9, D, X012
30D	79	D, D, C10, C9, D, P	35	1202	D, D, C10, C9, D, X012
31A	89	D, D, C10, C9, 70%, X012	38B	600	D, D, C10, C9, 70%, D
31B	159	D, D, C10, C9, D, X012	39A	771	D, D, C10, C9, D, X012A
31C	84	↓	39B	185	D, X020, C11, C10, X027, D
31D	372	↓	39C	415	D, X020, C11, C10, X027, D
31E	0	D, D, C10, C9, 70%, X012	40A	443	X072, D, C10, C9, D, X012A
31F	413	↓	40B	924	X072, D, C10, C9, D, X012A
31G	111	↓	41A	961	X072, D, C10, C9, D, D
32A	852	↓	41B	157	X072, D, C10, C9, D, D
32B	249	↓	42A	1344	X072, D, C10, C9, D, X079
32C	72	D, D, C10, C9, D, X012			
32D	224	D, D, C10, C9, D, X012			
33A	600	D, D, C10, C9, 70%, X012			

[a] C = control; D = driver; P = half driver fuel, half stainless steel; 70% = 70% enriched driver.

NOTE: X040A in position 5B4 during runs 39B and 39C; in 5B2 during all other runs.

The choice of representative X-Y configurations in this case was based upon the runs for which transport-theory calculations were available, changes of adjacent subassemblies, and variations in the measured reactivity worths of adjacent control rods. Results are shown in Table XIII. Runs 33B-35 were identified with run 40A rather than with run 32D or 38B on the basis of global variations in flux from run to run, as determined from measured reactivity worths of adjacent control rods No. 9 and 10. These worths in runs 33B-35 differed appreciably from the corresponding worths in runs 32D and 38B, but agreed closely with the worths in run 40A.

TABLE XIII. Representative X-Y Configurations for Subassembly X040A

Runs	MWd	Residence Fraction	Representative Configuration	Runs	MWd	Residence Fraction	Representative Configuration
30A-31G	2177	0.1690	31F	39A	771	0.0598	39A
32A-33A	1997	0.1550	32D	39B, 39C	600	0.0466	39C
33B-35	2910	0.2258	40A	40A, 40B	1367	0.1061	40A
38B	600	0.0466	38B	41A-42A	2462	0.1911	42A

2. X-Y Transport-theory Calculations

The X-Y transport-theory calculations for configurations in runs 31F, 32D, 38B, 39A, 39C, 40A, and 42A were all done in the S_2 approximation with the six-group ANL-23806 cross-section set.[12] Peak absolute fluxes and fission densities for the pertinent positions are given in Table XIV.

TABLE XIV. Peak Absolute Fluxes and Fission Rates for Subassembly X040A in Runs 31F, 32D, 38B, 39A, 39C, 40A, and 42A

Run (nominal power, MWt)	Position (X,Y)	Midplane Flux in Group x 10^{-14}							Fission Rates ($\Sigma\sigma_{fj}\phi_j$) x 10^9			
		Group 1: E_L = 2.23 MeV	Group 2: E_L = 821 keV	Group 3: E_L = 302 keV	Group 4: E_L = 111 keV	Group 5: E_L = 40.9 keV	Group 6: E_L = 29 eV	$\sum\phi_j$ x 10^{-15}	^{235}U	^{238}U	^{239}Pu	^{240}Pu
31F	19,30	1.762	4.131	6.116	4.812	2.003	0.7214	1.954	2.751	0.1840	3.254	1.280
(50);	20,30	1.836	4.253	6.267	4.919	2.040	0.7341	2.005	2.820	0.1907	3.339	1.320
Uranium	20,29	1.991	4.665	6.756	5.237	2.138	0.7626	2.155	3.023	0.2078	3.592	1.436
blanket	19,29	2.004	4.646	6.668	5.131	2.087	0.7293	2.126	2.977	0.2082	3.547	1.430
32D	19,30	1.757	4.088	6.062	4.811	2.024	0.7415	1.948	2.748	0.1829	3.243	1.271
(50);	20,30	1.755	4.135	6.219	4.936	2.067	0.7534	1.986	2.802	0.1836	3.304	1.286
Uranium	20,29	1.933	4.562	6.707	5.258	2.169	0.7860	2.141	3.012	0.2024	3.566	1.409
blanket	19,29	1.938	4.513	6.578	5.132	2.119	0.7583	2.103	2.955	0.2017	3.505	1.394
38B	19,30	1.848	4.267	6.192	4.798	2.004	0.7365	1.984	2.791	0.1917	3.309	1.319
(50);	20,30	1.814	4.243	6.244	4.883	2.041	0.7532	1.998	2.814	0.1892	3.328	1.314
Uranium	20,29	2.086	4.820	6.818	5.175	2.117	0.7531	2.177	3.047	0.2164	3.642	1.478
blanket	19,29	2.121	4.811	6.715	5.077	2.075	0.7316	2.153	3.010	0.2183	3.599	1.476
39A	19,30	1.750	4.120	6.094	4.800	2.018	0.7534	1.953	2.755	0.1831	3.252	1.457
(50);	20,30	1.769	4.156	6.169	4.879	2.051	0.7628	1.978	2.792	0.1849	3.293	1.289
Uranium	20,29	1.930	4.580	6.678	5.209	2.156	0.7957	2.135	3.004	0.2026	3.557	1.410
blanket	19,29	1.935	4.539	6.573	5.100	2.107	0.7666	2.102	2.953	0.2021	3.504	1.397
39C	23,30	1.677	4.040	6.121	4.971	2.143	0.8404	1.979	2.812	0.1772	3.289	1.256
(50);	24,30	1.632	3.875	5.871	4.848	2.120	0.8494	1.919	2.736	0.1714	3.189	1.210
Uranium	24,29	1.881	4.413	6.435	5.119	2.172	0.8259	2.084	2.946	0.1965	3.472	1.304
blanket	23,29	1.785	4.378	6.582	5.270	2.229	0.8551	2.110	2.987	0.1901	3.507	1.351
40A	19,30	1.690	3.897	5.906	4.759	2.025	0.8016	1.908	2.706	0.1752	3.173	1.222
(50);	20,30	1.699	3.955	6.075	4.901	2.072	0.8077	1.951	2.766	0.1769	3.242	1.243
Uranium	20,29	1.871	4.405	6.607	5.206	2.159	0.8270	2.107	2.974	0.1957	3.507	1.391
blanket	19,29	1.927	4.421	6.496	5.075	2.102	0.7935	2.081	2.932	0.1993	3.469	1.374
42A	19,30	1.690	3.897	6.153	4.888	2.072	0.8156	1.9858	2.811	0.1862	3.306	1.290
(50);	20,30	1.699	3.955	6.327	5.040	2.118	0.8194	2.0224	2.862	0.1850	3.362	1.298
Uranium	20,29	1.871	4.405	6.919	5.316	2.191	0.8273	2.2024	3.097	0.2113	3.672	1.463
blanket	19,29	1.927	4.421	6.778	5.191	2.141	0.8006	2.1723	3.050	0.2143	3.626	1.462

The normal ^{235}U enrichment in a Mark-IA driver-fuel subassembly is about 52%. In some runs, however, special subassemblies containing driver fuel with up to 70% enrichment were placed in the 4B1 position,

next to X040A. The question has arisen of whether the presence of driver fuel with such a high enrichment next to X040A may have increased the power generation in X040A significantly. The ^{235}U fission rate per atom at a point is a measure of the total power generation at that point. As Fig. 11 shows, a driver subassembly with 70%-enriched fuel was adjacent to X040A in runs 31F and 38B. Comparing ^{235}U fission rates per atom in runs 38B and 39A indicates that the adjacent 70%-enriched driver subassembly increases the power generation in subassembly X040A a maximum of only about 2%. It is thus concluded that an adjacent 70%-enriched driver had a small effect on the power generation in X040A.

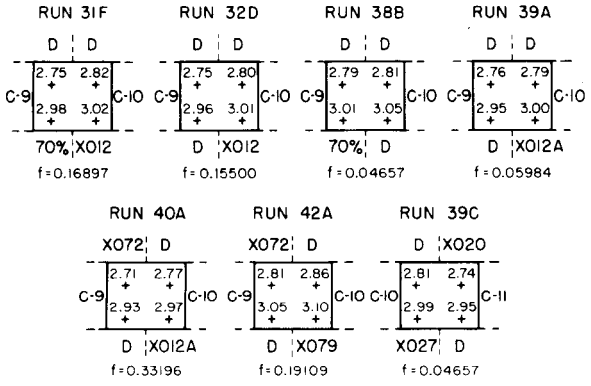

Fig. 11

Uranium-235 Fission Rates per Atom ($\times 10^9$) in Subassembly X040A during Seven Representative EBR-II Runs

3. Relative Axial Distributions

The axial distributions of total flux and fission densities at a given radius out to and including row 5 of EBR-II have changed very little from run to run since about run 30A. Therefore, for subassembly X040A the relative axial distributions were obtained from an R-Z transport-theory calculation on a single configuration, run 31F. The calculation was done in the S_2 approximation with the 22-group ANL-238 cross-section set.[12] Results are summarized in Fig. 12, which shows the differences between the distributions, and in Table XV, which gives the results at the midpoints of each of 20 equal axial nodes.

4. Element F3B3

Element F3B3 was at the center of subassembly X040A (position 19 in Fig. 3). The peak total flux in F3B3 in each representative X-Y configuration was thus taken as the average of the four values for the configuration given in Table XIV. These averages were then weighted for megawatt-days by using the residence fractions given in Table XIII. The axial distribution of absolute total flux was obtained by multiplying the averaged peak value by the relative axial distribution given in Table XV. The axial distributions of fission densities for the four heavy nuclides was computed in a similar manner, the method of Appendix A being used to account for burnup. The axial distribution of power in this element was based upon 191.4 MeV/fission, as determined from calculations given in Appendix C. Results are shown in Table XVI.

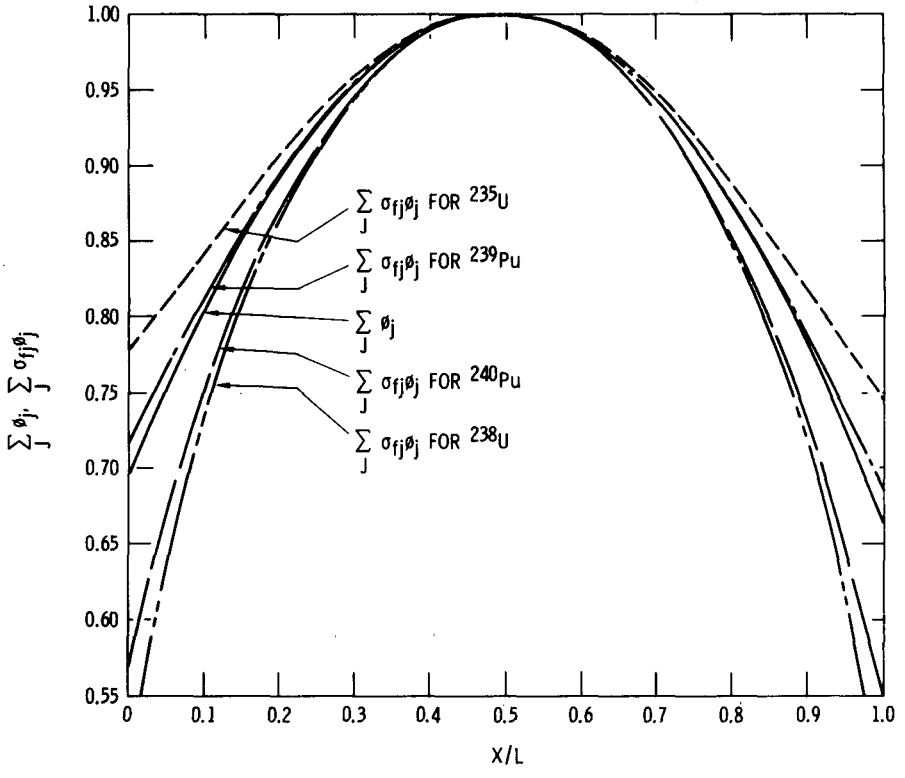

Fig. 12. Axial Distribution of Total Flux and Fission Densities for ^{235}U, ^{238}U, ^{239}Pu, and ^{240}Pu: Run 31F

TABLE XV. Axial Distributions of Total Flux and Fission Densities for Positions 5B2 (and 5B4), Run 31F

Axial Position above Core Bottom	$\frac{\sum_J \varphi_j(k)}{\sum_J \varphi_{j,max}}$ [a]	$\frac{\sum_J \sigma_{fj}^{235}\varphi_j(k)}{\sum_J \sigma_{fj}^{235}\varphi_{j,max}}$	$\frac{\sum_J \sigma_{fj}^{238}\varphi_j(k)}{\sum_J \sigma_{fj}^{238}\varphi_{j,max}}$	$\frac{\sum_J \sigma_{fj}^{239}\varphi_j(k)}{\sum_J \sigma_{fj}^{239}\varphi_{j,max}}$	$\frac{\sum_J \sigma_{fj}^{240}\varphi_j(k)}{\sum_J \sigma_{fj}^{240}\varphi_{j,max}}$
k = 1	0.7245	0.7928	0.572	0.7384	0.618
2	0.7789	0.8230	0.685	0.7860	0.709
3	0.8288	0.8567	0.772	0.8327	0.786
4	0.8720	0.8901	0.836	0.8740	0.841
5	0.9079	0.9200	0.881	0.9092	0.888
6	0.9385	0.9462	0.925	0.9393	0.927
7	0.9648	0.9686	0.958	0.9654	0.958
8	0.9832	0.9851	0.980	0.9833	0.980
9	0.9945	0.9955	0.994	0.9946	0.994
10	1.0000	1.0000	1.000	1.0000	1.000
11	0.9988	0.9992	0.999	0.9989	0.999
12	0.9918	0.9920	0.991	0.9914	0.992
13	0.9765	0.9791	0.975	0.9777	0.975
14	0.9553	0.9601	0.950	0.9561	0.950
15	0.9282	0.9353	0.917	0.9288	0.918
16	0.8940	0.9054	0.874	0.8948	0.878
17	0.8551	0.8729	0.824	0.8573	0.828
18	0.8082	0.8362	0.757	0.8122	0.767
19	0.7565	0.7989	0.668	0.7628	0.694
20	0.6980	0.7633	0.554	0.7113	0.598

[a] $\varphi_{j,max} \equiv \varphi_j(10)$.

TABLE XVI. Axial Distributions of Total Flux and Power in Element F3B3 in Subassembly X040A

Axial Node	$\phi_{total} \times 10^{-15}$	^{235}U Weight, g At t = 0	^{235}U Weight, g At Midlife	^{235}U $\frac{N_0}{A}\sum_J \sigma_{fj}\phi_j$, fiss/sec-g $\times 10^{-13}$	^{235}U Midlife Fission Rate, fiss/sec $\times 10^{-13}$	^{238}U Weight, g At t = 0	^{238}U Weight, g At Midlife	^{238}U $\frac{N_0}{A}\sum_J \sigma_{fj}\phi_j$, fiss/sec-g $\times 10^{-12}$	^{238}U Midlife Fission Rate, fiss/sec $\times 10^{-13}$	^{239}Pu Weight, g At t = 0	^{239}Pu Weight, g At Midlife	^{239}Pu $\frac{N_0}{A}\sum_J \sigma_{fj}\phi_j$, fiss/sec-g $\times 10^{-13}$	^{239}Pu Midlife Fission Rate, fiss/sec $\times 10^{-13}$	^{240}Pu Weight, g At t = 0	^{240}Pu Weight, g At Midlife	^{240}Pu $\frac{N_0}{A}\sum_J \sigma_{fj}\phi_j$, fiss/sec-g $\times 10^{-13}$	^{240}Pu Midlife Fission Rate, fiss/sec $\times 10^{-13}$	Total Fission Rate, fiss/sec $\times 10^{-13}$	Power,[a] Btu/hr
1[b]	1.4840	3.1543	3.0765	0.58627	1.80364	0.2592	0.2592	0.2793	0.00724	1.0321	1.0041	0.63751	0.64012	0.0101	0.0101	0.209	0.00210	2.45310	2567
2	1.5954	3.1543	3.0735	0.60861	1.87056	0.2592	0.2592	0.3345	0.00867	1.0321	1.0022	0.67861	0.68016	0.0101	0.0101	0.239	0.00242	2.56181	2681
3	1.6976	3.1543	3.0702	0.63353	1.94506	0.2592	0.2592	0.3769	0.00977	1.0321	1.0005	0.71893	0.71930	0.0101	0.0101	0.265	0.00268	2.67681	2801
4	1.7861	3.1543	3.0669	0.65823	2.01873	0.2592	0.2592	0.4082	0.01058	1.0321	0.9990	0.75459	0.75380	0.0101	0.0101	0.284	0.00287	2.78598	2916
5	1.8596	3.1543	3.0640	0.68034	2.08454	0.2592	0.2592	0.4302	0.01115	1.0321	0.9976	0.78498	0.78311	0.0101	0.0101	0.300	0.00303	2.88183	3016
6	1.9223	3.1543	3.0614	0.69971	2.14209	0.2592	0.2592	0.4516	0.01171	1.0321	0.9965	0.81096	0.80810	0.0101	0.0101	0.313	0.00316	2.96506	3103
7	1.9762	3.1543	3.0592	0.71628	2.19124	0.2592	0.2592	0.4678	0.01212	1.0321	0.9955	0.83350	0.82974	0.0101	0.0101	0.323	0.00326	3.03636	3178
8	2.0138	3.1543	3.0576	0.72848	2.22739	0.2592	0.2592	0.4785	0.01240	1.0321	0.9948	0.84895	0.84454	0.0101	0.0101	0.331	0.00334	3.08767	3231
9	2.0370	3.1543	3.0566	0.73617	2.25015	0.2592	0.2592	0.4853	0.01258	1.0321	0.9944	0.85871	0.85388	0.0101	0.0101	0.335	0.00339	3.12000	3265
10	2.04825	3.1543	3.0561	0.739496	2.25999	0.2592	0.2592	0.48826	0.01266	1.0321	0.99417	0.86337	0.85834	0.0101	0.0101	0.33742	0.00341	3.13440	3280
11	2.0458	3.1543	3.0562	0.73890	2.25822	0.2592	0.2592	0.4878	0.01264	1.0321	0.9942	0.86242	0.85743	0.0101	0.0101	0.337	0.00340	3.13169	3277
12	2.0315	3.1543	3.0569	0.73358	2.24248	0.2592	0.2592	0.4839	0.01254	1.0321	0.9945	0.85595	0.85124	0.0101	0.0101	0.335	0.00338	3.10964	3254
13	2.0001	3.1543	3.0582	0.72404	2.21424	0.2592	0.2592	0.4761	0.01234	1.0321	0.9950	0.84412	0.83992	0.0101	0.0101	0.329	0.00332	3.06982	3213
14	1.9567	3.1543	3.0600	0.70999	2.17259	0.2592	0.2592	0.4639	0.01202	1.0321	0.9958	0.82547	0.82204	0.0101	0.0101	0.321	0.00324	3.00989	3150
15	1.9012	3.1543	3.0625	0.69165	2.11816	0.2592	0.2592	0.4477	0.00161	1.0321	0.9969	0.80190	0.79939	0.0101	0.0101	0.310	0.00313	2.93229	3069
16	1.8311	3.1543	3.0654	0.66954	2.05241	0.2592	0.2592	0.4267	0.01106	1.0321	0.9982	0.77254	0.77112	0.0101	0.0101	0.296	0.00299	2.83758	2970
17	1.7515	3.1543	3.0686	0.64551	1.98081	0.2592	0.2592	0.4023	0.01043	1.0321	0.9996	0.74017	0.73986	0.0101	0.0101	0.279	0.00282	2.73392	2861
18	1.6554	3.1543	3.0722	0.61837	1.89976	0.2592	0.2592	0.3696	0.00958	1.0321	1.0013	0.70123	0.70214	0.0101	0.0101	0.259	0.00262	2.61410	2736
19	1.5495	3.1543	3.0759	0.59078	1.81716	0.2592	0.2592	0.3262	0.00845	1.0321	1.0032	0.65858	0.66067	0.0101	0.0101	0.234	0.00236	2.48864	2604
20	1.4297	3.1543	3.0794	0.56446	1.73817	0.2592	0.2592	0.2705	0.00701	1.0321	1.0051	0.61412	0.61727	0.0101	0.0101	0.202	0.00204	2.36449	2475

[a]Based upon 191.4 MeV/fission.
[b]Bottom of core.

5. Element 011

Element 011 was in position 21 of X040A (see Fig. 3). Its peak total flux and fission densities were taken from the values at the point (20,29) in the representative X-Y configurations for runs 31F, 32D, 38B, 39A, 40A, and 42A, and from the point (24,29) in the run-39C configuration. The values for each representative configuration were weighted for megawatt-days by using the residence fractions of Table XIII. Relative axial distributions were taken from Table XV, and total midlife fission densities were converted to Btu/hr of power on the basis of 191.4 MeV/fission. Results are summarized in Table XVII.

TABLE XVII. Axial Distributions of Total Flux and Power in Element 011 in Subassembly X040A

Axial Node	ϕ_{total} x 10^{-15}	Total Fission Rate, fissions/sec x 10^{-13}	Power,[a] Btu/hr	Axial Node	ϕ_{total} x 10^{-15}	Total Fission Rate, fissions/sec x 10^{-13}	Power,[a] Btu/hr
k = 1[b]	1.553	0.0	0.0	k = 11[b]	2.140	2.9533	3091
2	1.669	1.2555	1314	12	2.125	2.9326	3069
3	1.776	2.5280	2646	13	2.093	2.8951	3030
4	1.869	2.6297	2752	14	2.047	2.8391	2971
5	1.946	2.7193	2846	15	1.989	2.7663	2895
6	2.011	2.7972	2927	16	1.916	2.6777	2802
7	2.068	2.8639	2997	17	1.832	2.5806	2701
8	2.107	2.9120	3048	18	1.732	1.4814	1550
9	2.131	2.9424	3079	19	1.621	0.0	0.0
10	2.143	2.9558	3093	20	1.496	0.0	0.0

[a]Based upon 191.4 MeV/fission.
[b]Bottom of core.

IV. CONCLUSIONS

In the calculation of axial distributions of flux and power in mixed-oxide subassemblies irradiated in EBR-II, account should be taken of the following effects:

1. Global and local variations in flux in the reactor on a run-to-run basis.
2. Burnup of heavy nuclides.
3. The factor used to convert total fission rate to power.

Flux and fission densities from a cylindrical-geometry, transport-theory calculation on one EBR-II configuration (such as that given in the Guide for Irradiation Experiments in EBR-II[4]) cannot even account for global or local variations in flux that occur in that run. A detailed understanding of such variations over several runs requires X-Y or equivalent transport-theory calculations to be made at least every few runs and ideally every run.

In the calculation of the midlife axial power distribution in a mixed-oxide element irradiated to about 10% peak burnup in EBR-II, the axial variation of burnup of ^{235}U and ^{239}Pu had to be considered. The burnup of ^{238}U was neglected because it was small, and the burnup of ^{240}Pu was neglected because of its low initial mass. Calculations indicated that at about 10% peak burnup, conversion of ^{238}U to ^{239}Pu was negligible, as was the conversion of ^{239}Pu to ^{240}Pu.

The axial distribution of the effective MeV/fission was calculated for two UO_2-20% PuO_2 mixed-oxide elements that were irradiated in EBR-II. One element was in a 19-element subassembly in row 4; the other was in a 37-element subassembly in row 5. With 20 axial nodes being used, the effective MeV/fission for the row-4 element was found to vary only between 188.7 and 191.0, with 15 of the 20 values falling within 0.105% of 190.8. For the row-5 element, the variation was from 189.0 to 191.5, with 14 of the 20 values falling within 0.052% of 191.4. Thus, for UO_2-20% PuO_2 oxide subassemblies in rows 1-5 of EBR-II, total fission rates apparently can be converted to power by using a constant factor of about 191 MeV/fission.

Normal EBR-II driver fuel is about 52% enriched in ^{235}U. During some runs, however, a special type of driver subassembly containing elements with 70% enriched fuel was placed next to subassembly X040A. A question arose as to whether the presence of a 70%-enriched driver next to X040A caused an increase in the power generation in X040A. Examination of ^{235}U fission-density distributions from X-Y transport-theory calculations for seven representative runs showed a maximum power increase in X040A of about 2%. The special subassembly did not significantly increase power generation in X040A.

Finally, the methods presented here can be computerized to serve as an interface between two-dimensional transport-theory calculations and two-dimensional heat-transfer calculations, either on a run-to-run basis, or on an appropriate average basis. Resulting detailed distributions of flux and temperature would be of great importance in interpreting results of irradiation experiments in EBR-II.

APPENDIX A

A Derivation of Equations for Burnup of Heavy Atoms

(See Nomenclature)

The total irradiation time t is given by

$$t = (24)(3600) \sum_{N} M_i/P_i \text{ sec.} \tag{A.1}$$

The absolute fission density of nuclide m in axial node k is

$$r_m(k) = \frac{N_0}{A_m} \sum_{J} \sigma_{fj}^{m} \varphi_j(k) \frac{\text{fissions}}{\text{g-sec}}. \tag{A.2}$$

In time t, the total number of fissions in 1 g of nuclide m in axial node k is

$$r_m(k)t = \frac{N_0 t}{A_m} \sum_{J} \sigma_{fj}^{m} \varphi_j(k) \frac{\text{fissions}}{\text{g}}. \tag{A.3}$$

The weight (grams) of nuclide m "burned" per initial gram of nuclide m in axial node k is

$$\beta_{ml}(k) = \frac{N_0 t}{A_m} \sum_{J} \sigma_{fj}^{m} \varphi_j(k) \frac{\text{fissions}}{\text{initial g}} \times \frac{\text{1 burned atom}}{\text{fission}} \times \frac{\text{1 mole burned atoms}}{N_0 \text{ burned atoms}}$$

$$\times \frac{A_m \text{ g burned}}{\text{1 mole burned atoms}} = t \sum_{J} \sigma_{fj}^{m} \varphi_j(k) \frac{\text{g burned}}{\text{initial g}}. \tag{A.4}$$

However, this value must be corrected for the decrease in nuclide m with time. Assume a midlife burnup of

$$0.5t \sum_{J} \sigma_{fj}^{m} \varphi_j(k).$$

The ratio of average density to initial density of nuclide m is approximately

$$1 - 0.5 \sum_{J} \sigma_{fj}^{m} \varphi_j(k),$$

and the second iteration on the burnup is

$$\beta_{m2}(k) = \left[1 - 0.5t \sum_J \sigma_{fj}^m \varphi_j(k)\right] t \sum_J \sigma_{fj}^m \varphi_j(k). \quad (A.5)$$

The third iteration is

$$\beta_{m3}(k) = \left\{1 - 0.5\left[1 - 0.5t \sum_J \sigma_{fj}^m \varphi_j(k)\right] t \sum_J \sigma_{fj}^m \varphi_j(k)\right\} t \sum_J \sigma_{fj}^m \varphi_j(k). \quad (A.6)$$

Continued iteration yields the infinite series

$$\beta_{m\infty}(k) = \left\{1 - \frac{t \sum_J \sigma_{fj}^m \varphi_j(k)}{2} + \left[\frac{t \sum_J \sigma_{fj}^m \varphi_j(k)}{2}\right]^2 - \ldots\right\} t \sum_J \sigma_{fj}^m \varphi_j(k)$$

$$= \left[1 + \frac{t \sum_J \sigma_{f1}^m \varphi_j(k)}{2}\right]^{-1} t \sum_J \sigma_{fj}^m \varphi_j(k)$$

$$= \left[1 + \frac{\beta_{m1}(k)}{2}\right]^{-1} \beta_{m1}(k).$$

But

$$\beta_{m1}(k) = \beta_{m1}(10) \frac{r_m(k)}{r_m(10)};$$

i.e.,

$$\beta_{m\infty}(k) = \left[1 + \frac{\beta_{m1}(10)}{2} \frac{r_m(k)}{r_m(10)}\right]^{-1} \beta_{m1}(10) \frac{r_m(k)}{r_m(10)}.$$

Note that the parameter $\beta_{m1}(10)$ is evaluated from results of transport-theory calculations in X-Y geometry, and the ratio $r_m(k)/r_m(10)$ is evaluated from transport-theory calculations in R-Z geometry. The total burnup in axial node k is approximately

$$BU(k) = \frac{\sum_{m=1}^{4} \beta_{m\infty}(k) W_m(k)}{\sum_{m=1}^{4} W_m(k)}, \qquad (A.7)$$

and the midlife mass of heavy nuclide m in axial node k is approximately

$$\overline{W_m(k)} = W_m(k)\left\{1 - \left[1 + \frac{\beta_{m1}(10)}{4} \frac{r_m(k)}{r_m(10)}\right]^{-1} \frac{\beta_{m1}(10)}{2} \frac{r_m(k)}{r_m(10)}\right\}. \qquad (A.8)$$

APPENDIX B

Effective MeV/fission for X012

The total midlife power deposition in axial node k, P(k), is given by

$$\frac{1}{K} P(k) = \sum_{m=1}^{4} E_m \overline{W_m(k)} r_m(k) + P_{\gamma h}(k) \sum_{m=1}^{4} \overline{W_m(k)} + P_{\gamma s}(k) W_s(k). \qquad (B.1)$$

Values of E_m are taken from the work of James,[14] and values of $P_{\gamma h}$ and $P_{\gamma s}$ are taken from representative distributions of gamma deposition used in Ref. 4. The effective MeV/fission is defined as

$$(\text{MeV/fission})_k = \frac{1}{K} P(k) \Big/ \sum_{m=1}^{4} \overline{W_m(k)} r_m(k). \qquad (B.2)$$

The effective MeV/fission for a given element thus depends upon the following:

1. Initial axial mass distributions of the heavy nuclides.
2. Residence time in EBR-II.
3. Axial mass distribution of the stainless steel.
4. Absolute axial distributions of fission densities for the heavy nuclides.
5. Total kinetic energy per fission for each of the heavy nuclides.
6. Absolute axial distributions of gamma-energy deposition in the heavy nuclides and the stainless steel.

Following is a calculation of the axial distribution of the effective MeV/fission for oxide fuel element C17 in subassembly X012. In this calculation, values of $\overline{W_m(k)}$ and $r_m(k)$ were taken directly from Table V. The values of $P_{\gamma h}$ and $P_{\gamma s}$ were normalized to a megawatt-day-averaged power (see Table II) of

$$45 \times \frac{8875}{18276} + 50 \times \frac{9401}{18276} = 47.57 \text{ MWt.}$$

Results are shown in Table XVIII. The effective MeV/fission in this element varies only from 188.7 to 191.0, and 15 of the 20 values lie within 0.105% of 190.8 MeV/fission.

TABLE XVIII. Effective MeV/fission for Element C17 in Subassembly X012

Axial Node	Kinetic Energy Deposition, Btu/hr					Weight of Heavy Atoms ($^{235}U + ^{238}U + ^{239}Pu + ^{240}Pu$), g	U + Pu Gamma Heating, $W/g \div \frac{47.57}{62.50}$	U + Pu Gamma Heating, Btu/hr	Stainless Steel[a] Gamma Heating		Total Power, Btu/hr	$(MeV/fission)_k$
	^{235}U	^{238}U	^{239}Pu	^{240}Pu	Total				$W/g \div \frac{47.57}{62.50}$	Btu/hr		
1	1542.05	7.25	458.64	10.72	2018.66	3.4531	10.40	93.29	3.79	10.78	2122.73	188.8
2	1605.11	8.58	486.53	11.95	2112.17	3.4469	12.40	111.03	4.73	13.45	2236.65	190.2
3	1667.70	9.74	513.51	13.07	2204.02	3.4407	13.60	121.55	5.23	14.88	2340.45	190.7
4	1729.60	10.69	539.18	14.10	2293.57	3.4346	14.40	128.47	5.51	15.67	2437.71	190.9
5	1789.65	11.38	561.61	15.01	2377.65	3.4289	14.96	133.25	5.74	16.33	2527.23	190.9
6	1840.65	11.93	580.81	15.73	2449.12	3.4241	15.44	137.33	5.93	16.87	2603.32	190.9
7	1881.81	12.37	595.56	16.24	2505.98	3.4202	15.84	140.73	6.09	17.32	2664.03	191.0
8	1912.57	12.70	607.89	16.65	2549.81	3.4171	16.12	143.09	6.21	17.66	2710.56	191.0
9	1932.91	12.89	614.66	16.85	2577.31	3.4152	16.31	144.69	6.28	17.86	2739.86	191.0
10	1940.31	12.97	617.79	17.06	2588.13	3.4145	16.41	145.55	6.31	17.95	2751.63	191.0
11	1939.04	12.96	617.08	16.95	2586.03	3.4147	16.41	145.56	6.29	17.89	2749.48	191.0
12	1932.52	12.67	607.08	16.65	2568.92	3.4146	16.30	144.58	6.25	17.78	2731.28	191.0
13	1934.37	11.79	577.17	15.83	2539.16	3.4117	16.01	141.89	6.15	17.49	2698.54	190.8
14	1896.02	11.47	564.84	15.32	2487.65	3.4153	15.70	139.29	6.02	17.12	2644.06	190.8
15	1849.70	11.05	548.37	14.71	2424.13	3.4196	15.24	135.37	5.86	16.67	2576.17	190.8
16	1794.03	10.52	528.87	14.10	2347.72	3.4249	14.71	130.87	5.63	16.01	2494.60	190.8
17	1726.77	9.83	506.24	13.28	2256.12	3.4311	14.09	125.58	5.38	15.30	2397.00	190.7
18	1655.72	8.94	478.65	12.26	2155.57	3.4379	13.20	117.88	5.05	14.36	2287.81	190.5
19	1585.06	7.86	449.75	11.13	2053.80	3.4447	11.90	106.48	4.59	13.06	2173.34	189.9
20	1512.65	6.77	421.26	9.81	1950.49	3.4517	10.10	90.56	3.60	10.24	2051.29	188.7

[a]The weight of stainless steel for all nodes was 1.095 g.

APPENDIX C

Effective MeV/fission for X040A

The method given in Appendix B for calculating the axial distribution of the effective MeV/fission is applied here to element F3B3 in subassembly X040A. Midlife fission rates and heavy-atom masses per axial node are taken from Table XVI. Gamma-heating values for the heavy isotopes and stainless steel are taken from representative distributions, used in Ref. 4, which are renormalized to reactor operation as 50 MWt. Results of the calculations (Table XIX) show that the effective MeV/fission for this element varies from 189.0 to 191.5. Here 14 of the 20 values lie within 0.052% of 191.4 MeV/fission.

TABLE XIX. Effective MeV/fission for Element F3B3 in Subassembly X040A

Axial Node	Kinetic Energy Deposition, Btu/hr					Weight of Heavy Atoms ($^{235}U + ^{238}U + ^{239}Pu + ^{240}Pu$), g	U + Pu Gamma Heating, W/g ÷ 50/62.50	U + Pu Gamma Heating, Btu/hr	Stainless Steel[a] Gamma Heating		Total Power, Btu/hr	$\overline{(MeV/fission)}_k$
	^{235}U	^{238}U	^{239}Pu	^{240}Pu	Total				W/g ÷ 50/62.5	Btu/hr		
1	1755.43	7.05	646.81	2.14	2411.43	4.3499	9.13	108.43	3.31	15.87	2535.73	189.0
2	1820.56	8.45	687.27	2.47	2518.75	4.3450	11.08	131.44	4.17	19.99	2670.19	190.6
3	1893.07	9.52	726.82	2.74	2632.15	4.3400	12.09	143.26	4.61	22.10	2797.51	191.1
4	1964.77	10.31	761.68	2.93	2739.69	4.3352	12.81	151.63	4.89	23.44	2914.76	191.3
5	2028.82	10.86	791.29	3.09	2834.06	4.3309	13.32	157.51	5.09	24.40	3015.97	191.4
6	2084.83	11.41	816.54	3.23	2916.01	4.3272	13.73	162.22	5.27	25.27	3103.49	191.4
7	2132.66	11.81	838.41	3.33	2986.21	4.3240	14.12	166.70	5.41	25.94	3178.85	191.5
8	2167.85	12.08	853.36	3.41	3036.70	4.3217	14.36	169.44	5.49	26.32	3232.46	191.5
9	2190.00	12.26	862.80	3.46	3068.52	4.3203	14.55	171.63	5.56	26.66	3266.81	191.5
10	2199.58	12.34	867.31	3.48	3082.71	4.3196	14.61	172.31	5.60	26.85	3281.87	191.5
11	2197.85	12.32	866.39	3.47	3080.03	4.3197	14.59	172.08	5.59	26.80	3278.91	191.5
12	2182.53	12.22	860.13	3.45	3058.33	4.3207	14.49	170.94	5.54	26.56	3255.83	191.5
13	2155.05	12.02	848.70	3.39	3019.16	4.3225	14.28	168.53	5.46	26.18	3213.87	191.5
14	2114.51	11.71	830.63	3.31	2960.16	4.3251	13.98	165.09	5.35	25.65	3150.90	191.5
15	2061.54	11.31	807.74	3.20	2883.79	4.3287	13.57	160.38	5.21	24.98	3069.15	191.4
16	1997.55	10.78	779.18	3.05	2790.56	4.3329	13.09	154.86	5.01	24.02	2969.44	191.4
17	1927.86	10.16	747.59	2.88	2688.49	4.3375	12.58	148.98	4.78	22.92	2860.39	191.3
18	1848.98	9.33	709.48	2.68	2570.47	4.3428	11.78	139.68	4.50	21.57	2731.72	191.1
19	1768.58	8.23	667.57	2.41	2446.79	4.3484	10.80	128.22	4.12	19.75	2594.77	190.7
20	1691.71	6.83	623.72	2.08	2324.34	4.3538	8.90	105.80	3.21	15.39	2445.53	189.2

[a]*The weight of stainless steel for all nodes was 1.756 g.*

REFERENCES

1. S. D. Harkness and C. Y. Li, *A Model for Void Formation in Metals Irradiated in a Fast-neutron Environment*, ANL-7588 (Aug 1969).
2. R. D. Leggett *et al.*, *Correlation of Predictions and Observations in Mixed Oxide Fuel*, Trans. Am. Nucl. Soc. *13*(2), 574 (1970).
3. V. Z. Jankus and R. W. Weeks, *LIFE-I, A FORTRAN-IV Computer Code for the Prediction of Fast-reactor Fuel-element Behavior*, ANL-7736 (Nov 1970).
4. *Guide for Irradiation Experiments in EBR-II, Revision 4*, EBR-II Project Document (Feb 1971).
5. L. B. Miller and R. E. Jarka, *Asymmetry and Local Distortions of the Flux Due to Gross Heterogeneities in EBR-II*, Trans. Am. Nucl. Soc. *12*(2), 772 (1969).
6. L. B. Miller and R. E. Jarka, *Detailed Analysis of Space-dependent Phenomena*, Trans. Am. Nucl. Soc. *13*(1), 307 (1970).
7. R. R. Smith *et al.*, *The Effects of an Over-cooled Stainless Steel Reflector on the EBR-II Power Coefficient*, ANL-7544 (May 1969).
8. J. C. Case, *Core-loading Diagrams for EBR-II Runs 4 through 38 (April 1965 through mid-December 1969)*, ANL/EBR-007 (Dec 1969).
9. L. J. Koch, W. B. Loewenstein, and H. O. Monson, *Addendum to Hazard Summary Report: Experimental Breeder Reactor-II (EBR-II)*, ANL-5719 (Addendum) (June 1962).
10. J. C. Case, *Loading Diagrams of Experimental Subassemblies Irradiated in EBR-II Runs 5 through 42*, ANL/EBR-015 (May 1970).
11. G. H. Golden, *Elementary Neutronics Considerations in LMFBR Design*, ANL-7532 (Mar 1969).
12. J. T. Madell and R. E. Jarka, *Comparison of the Various Neutronic Representations for EBR-II Analyses*, ANL-7540 (Feb 1970).
13. T. D. Claar, Argonne National Laboratory, private communication (Dec 1970).
14. M. F. James, *Energy Released in Fission*, J. Nucl. Energy *23*, 517 (1969).